N63-18410

OTS PRICE

XEROX $

MICROFILM $

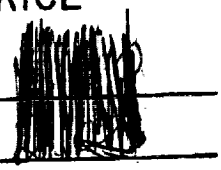

1st Quarterly Report
Period of 10 April to 10 July 1962

FUEL CELL ASSEMBLIES

Prepared for

Jet Propulsion Laboratory
California Institute of Technology
4800 Oak Grove Drive
Pasadena, California

Attn: Mr. J. McMahan
Contract No. JPL 950258

EOS Report 3070-Q-1

10 July 1962

Prepared by

Harvey Frank

Harvey Frank
Project Supervisor

Approved by

C.W. Stephens

C.W. Stephens
Acting Manager
Chemical Systems Department

Approved by

J. Neustein

J. Neustein, Manager
ADVANCED POWER SYSTEMS DIVISION

ELECTRO-OPTICAL SYSTEMS, INC. - PASADENA, CALIFORNIA

CONTENTS

CONTENTS (contd)

ILLUSTRATIONS

1. INTRODUCTION

This report describes the development of regenerative fuel cell assemblies that has been performed under Jet Propulsion Laboratory (JPL) Contract No. 950258 (EOS No. 3070) for the first quarter, 7 April to 7 July 1962.

The objective of the program is to develop and deliver three multi-cell regenerative hydrogen oxygen fuel cell assemblies to JPL. Specific objectives for the first quarter were to design and begin fabrication of the first prototype assembly, conduct supporting fuel cell investigations and carry out a heat transfer analysis for the first prototype, and finally to establish quality control specifications, test procedures, and fabrication techniques for subsequent models.

Overall progress in meeting the first quarter's objectives has been good, and the program for the second quarter will proceed according to the original schedule. Fabrication of the first prototype is nearing completion and will be ready for test in the early part of the second quarter. Processing procedures have been established for the fabrication of electrodes, electrolyte bed, and cell spacers. Tentative quality control specifications have been written for all materials. The proper sized manifolds, gas distribution channels, O-rings, and compression of the cell stack have been established by the supporting fuel cell investigations. Additional studies have established the best materials and provided some information on safety hazards.

The program for the second quarter will consist of testing the first prototype, establishing the necessary modifications or redesign, carrying out any required changes, and then retesting. No major problems are anticipated in making the fuel cell portion of the first prototype functional since the predicted performance of the proposed 6-inch diameter cells has already been proven on laboratory models. However, the heat

transfer analysis has indicated that the configuration selected for the first prototype does not provide adequate heat-transfer paths from the fuel cell. Therefore, it is anticipated that the major portion of the modifications and possible redesign will be concerned with heat transfer. Other modifications will be concerned with reducing the weight of the assembly. (The first prototype will weigh approximately 90 lbs and its corresponding energy-to-weight ratio will be slightly over 10 watt-hours per lb.

2. DESCRIPTION OF CELLS

Three types of cells are referred to in various sections of this report. A description of each of these cells is given below.

2.1 Small Experimental Cells

Figure 1 shows the components of a small experimental laboratory cell (1 5/8-inch diameter electrodes). The electrodes are platinized porous nickel 0.022-inch thick. The electrolyte is potassium hydroxide solution impregnated in a disc of asbestos 1/32-inch thick. The cell end plates are made of stainless steel and contain a silicon rubber O-ring to seal the gases. The miniature gas cylinders are also made of stainless steel and have volume ratios of 2/1 for H_2 and O_2 respectively.

2.2 Large Experimental Cells

The large experimental cells are essentially the same as the small. Electrode diameters of 4 inches and 6 inches were employed in these models. Series operation of the 6-inch diameter cells was accomplished by adding cell spacers (with provision for electrodes and gas manifolds) between the end plates. The spacers were similar to those of the prototype described below.

2.3 Prototype A

Prototype A is currently under fabrication and should be ready for test in late July. An assembly drawing of the unit is shown in Fig. 2.

The unit will contain 38 series connected cells, as shown in Fig. 2, that are held together and clamped to a large base plate by an insulated bolt. A Teflon bellows, which serves as a pressure equalizer, is suspended from the other side of the base plate. The whole assembly is enclosed in a pressure vessel that consists of stainless steel weld

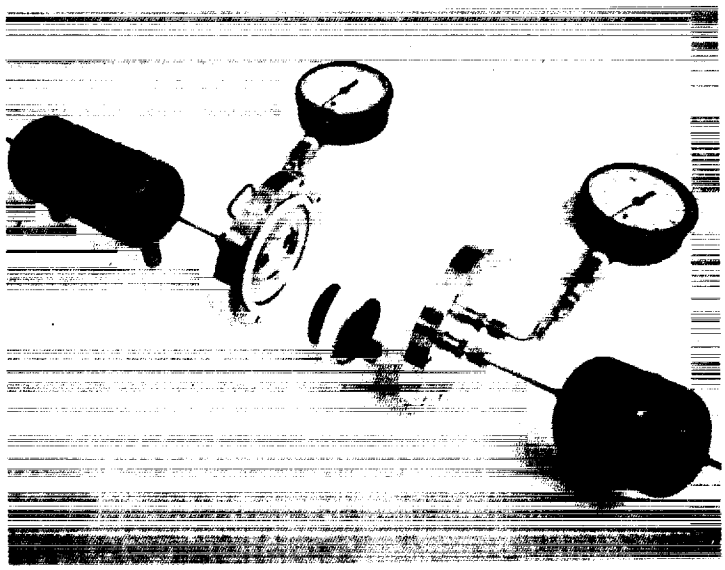

A. Hydrogen container
B. Oxygen container
C. Cell frame with "O" ring
D. Hydrogen electrode
E. Oxygen electrode
F. Pressure gages
G. Asbestos bed

FIG. 1 COMPONENTS OF SMALL LABORATORY CELL

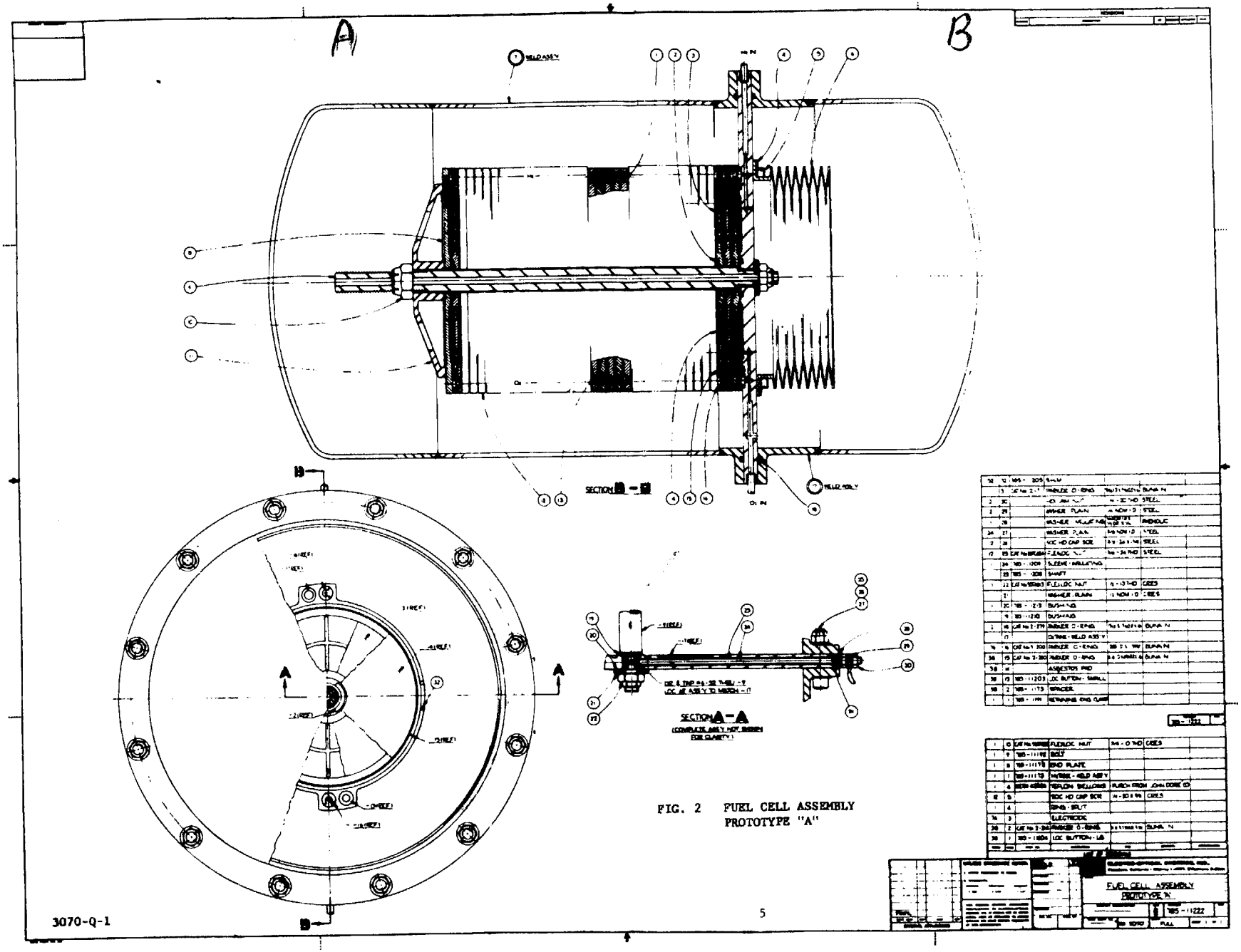

FIG. 2 FUEL CELL ASSEMBLY
PROTOTYPE "A"

3070-Q-1

caps and pipe. Hydrogen gas is stored in the annular space surrounding the fuel cell as well as inside the hollowed center bolt and bellows. Oxygen is stored in the annular space surrounding the bellows. Hydrogen flows from the storage chamber to the cells via a path starting at the inside of the bellows, through a hole in the base plate, and then to the main hydrogen manifold line. Oxygen flows from its storage chamber through a hole in the face plate to the main oxygen manifold.

A drawing of one of the unit cell spacers is shown in Fig. 3. The spacer is made of Plex 55, a high temperature grade of acrylic, and is coated with a metal layer consisting of silver, copper, and nickel. The function of the metal layer is to connect the cells in series as well as to conduct the heat. The spacer contains a recessed area for the electrodes, with deeper grooves within this recessed area to distribute the gases behind the electrode. Four O-rings are employed, two of which seal the manifold lines and two to seal the electrodes from the hydrogen chamber.

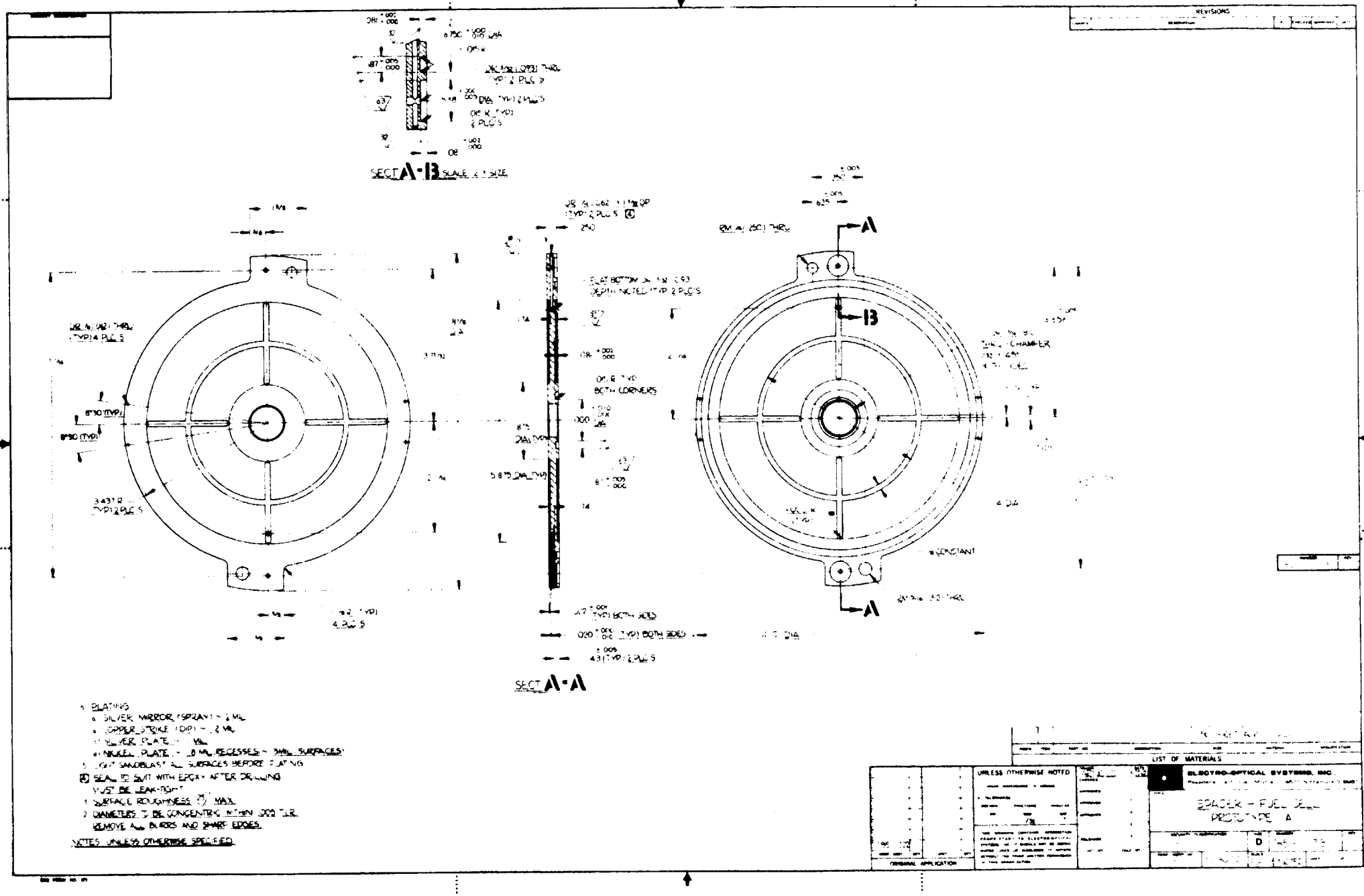

FIG. 3 SPACER - FUEL CELL PROTOTYPE "A"

3. FUEL CELL INVESTIGATION

This section gives the results of experimental investigations on the fuel cell portion of the proposed units.

3.1 Voltage-Current Characteristics

The discharge voltage-current characteristics for 6-inch diameter electrodes (the size to be employed in the final units) were determined for a single cell at two temperatures, and for three cells in series at one temperature. The results are given below.

Single Cell at 50 psig

Amps	ma/cm^2	Volts at 70^oF	Volts at 150^oF
0	0	1.04	1.04
0.5	2.7	.93	.94
1.0	5.5	.88	.91
2.0	11.0	.81	.89
5.0	27.3	.63	.82
10.0	54.5	-	.73

Three Cells in Series at 70^oF

Amps	ma/cm^2	Volts
0	0	3.05
0.5	2.7	2.80
1.0	5.5	2.72
2.0	11.0	2.55
5.0	27.3	2.06

The above results are in accord with the corresponding data for the smaller experimental cells (1 5/8-inch diameter and 4-inch diameter) and indicate no effect of scaling to this size.

3.2 Compression

The voltage-current characteristics of a cell with 6-inch diameter electrodes were measured as a function of the amount of compression of the electrolyte layer (KOH impregnated asbestos). The results indicated

that the cell performance was high and independent of compression of from 38 to 53 percent (25 to 35 mils) of the original asbestos thickness of 66 mils. The cell discharge voltage at 2.0 amps was, for example, 0.840 volts for 25 mils compression and 0.845 volts for 35 mils compression.

3.3 Manifold Diameter

Voltage-time tests indicate that the minimum manifold diameter for cells with 6-inch diameter electrodes is 3/32 inch. With this size manifold the discharge voltage is constant with time at currents up to at least 11.0 amps. With 1/16-inch diameter manifolds on the other hand, voltage was found to drift to zero in a matter of minutes at 9.0 amps.

3.4 Electrode Studies

Three types of investigations were carried out on the porous nickel electrodes. Two of these investigations were concerned with the platinization procedures and one with the quality of the raw material.

3.4.1 Platinum Content

At the start of this program the electrode platinization procedure called for the deposition of 40 mg Pt/in^2 on both hydrogen and oxygen electrodes. However, subsequent investigations indicated that although this platinum content is required on the hydrogen electrode for good cell performance, the same amount is not required on the oxygen electrode for the same cell performance. Subsequently a set of electrodes was prepared with 40 mg/in^2 on the hydrogen electrode and 20 mg/in^2 on the oxygen electrode. The results indicated that the cell performance was nearly identical with that of a cell containing 40 mg/in^2 on both electrodes; that is, 15 ma/in^2 at 0.80 volts at room temperature. Since the same performance can be obtained with less platinum, and correspondingly reduced cost, the electrode platinization procedures will be modified to deposit 20 mg Pt/in^2 on the oxygen electrode.

3.4.2 Reproducibility of Plating

In order to test the reproducibility of the platinization procedures, ten electrodes (4-inch diameter) were prepared and run against

a common hydrogen electrode. On discharge at 1.0 amp the cell voltage was 0.77 ± 0.06 volts for all ten electrodes. The results indicate that the electrodes can be platinized in such a manner that the resultant activities (as measured by discharge voltage) vary with ± 8 percent. Since other factors (see below) may have accounted for some of this variation, this value is a maximum that may be attributed to the platinization procedures.

3.4.3 Porosity of Plates

A verbal report from the supplier of the porous nickel plates, Gould National Batteries, indicated appreciable variation of porosity of the plates (74 to 87 percent). Subsequent examination of a shipment of fifty of these 7 x 7-inch plates established variations of from 77.3 to 79.6 percent. Of these fifty electrodes the two with extreme variations in porosity were sorted out and are currently under test. The first test results indicate that the voltage-current characteristics appear to be a strong function of the porosity.

3.5 Safety Investigations

If an external gas leak should suddenly occur in either the H_2 of O_2 cylinders, the gas from the other cylinder would break through the asbestos bed and result in the mixing of the two gases. Mixing could also be brought about by a failure of the Teflon diaphragm or one of the cell spacers.

With these possibilities of mixing the question arises as to potential safety hazards in the operation of the cell. Based on the fact that the auto-ignition temperature of hydrogen in air is 1076°F, with explosive limits of 4.1 to 74.2 percent, and the maximum operating cell temperature is 200°F, it would appear unlikely at first glance that an explosion could occur. However, it should be pointed out that since pure oxygen is present instead of air, and since a platinum catalyst is also present, the auto-ignition temperature could be appreciably reduced. Under these considerations the following tests were carried out:

Test No. 1 - 80 percent H_2 - 20 percent O_2

A small gas cylinder, 240 cc, was pressurized first with 80 psi of H_2 and then with 20 psi of O_2. A valve was then opened to permit the gas mixture to come in contact with one side of a cell containing the platinized-nickel electrode. The gas pressure and cell temperature were recorded, and the following observations were made:

1. No explosion occurred.
2. The gas pressure declined slowly from 100 psig to 5 psig in 2 days.
3. The temperature rise was negligible - less than $1^{\circ}F$ above room temperature.

These results indicate that the gases do react, but very slowly, on the platinum electrode.

Test No. 2 - 20 percent H_2 - 80 percent O_2

The same test was repeated but in this case the cylinder was pressurized first with 20 psi of H_2 and then with 80 psi of O_2. Similar results were obtained.

3.6 Corrosion Studies

Since the chemical environment within the fuel cell is very conducive to corrosion, a number of tests were carried out to determine the suitability of the proposed as well as alternative materials of construction. The tests consisted of wrapping the sample in KOH impregnated asbestos (simulating the strong basic electrolyte), placing it in a steel vessel, pressurizing with oxygen at 100 psig, and heating at $125^{\circ}C$ for 24 hours (see Fig. 4). Sample weights and visual observations were made before and after the tests. Results are given below.

Material	Initial Weight grams	Final Weight grams	Observations
Nickel	-	-	No change
301 Stainless	0.42	0.42	Moderate surface oxidation
302 Stainless	0.65	0.65	Heavy surface oxidation
304 Stainless	-	-	Heavy surface oxidation

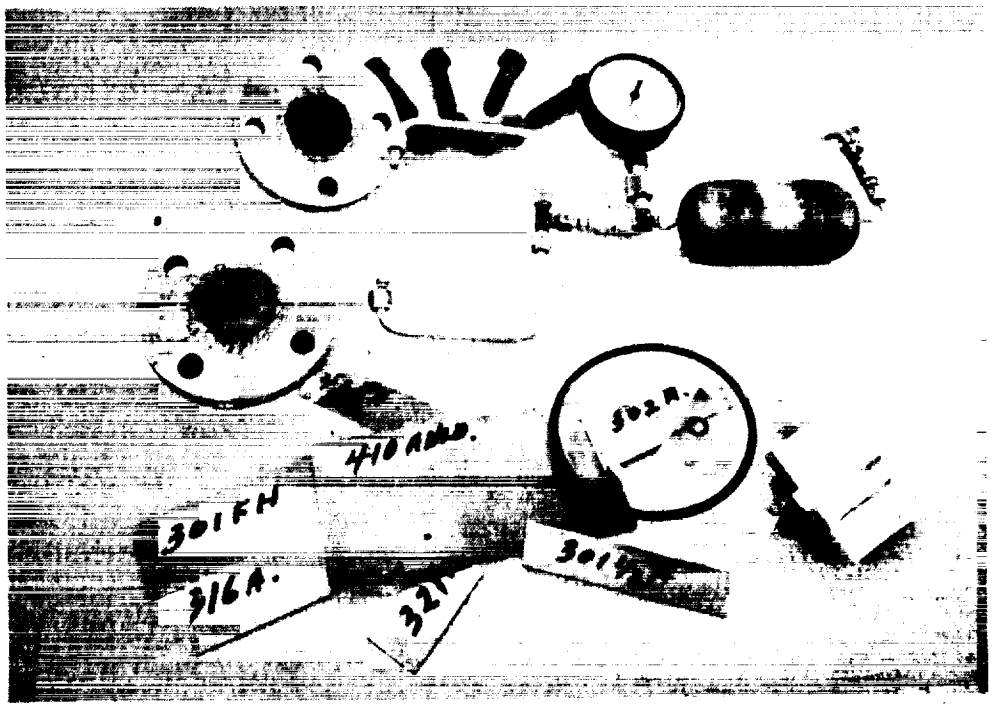

FIG. 4 APPARATUS FOR CORROSION TESTS

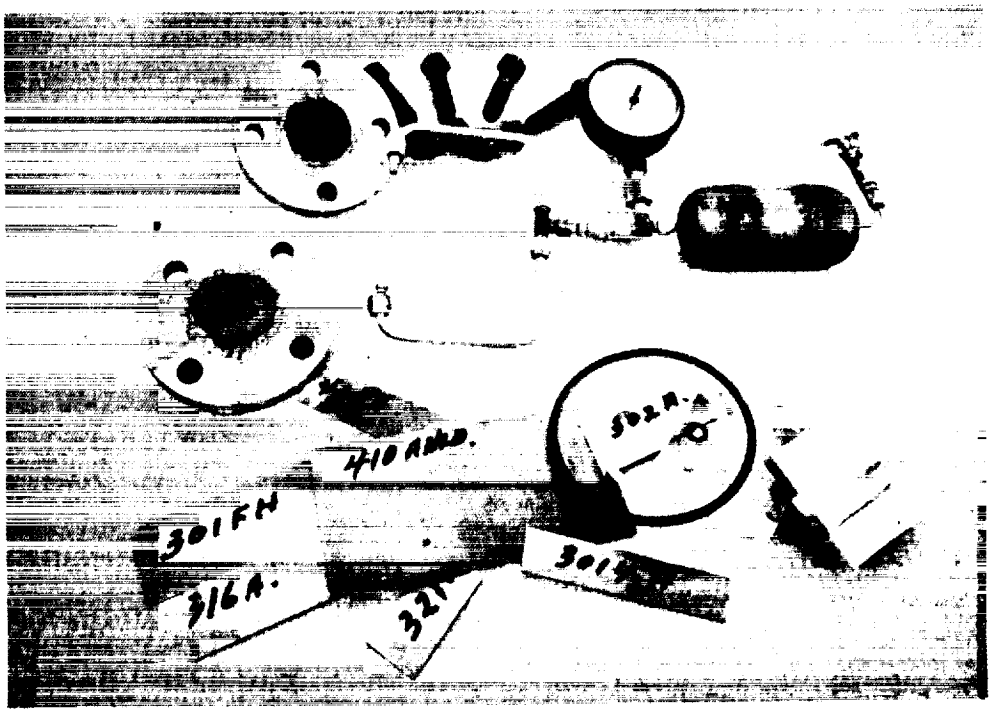

FIG. 4 APPARATUS FOR CORROSION TESTS

Material	Initial Weight grams	Final Weight grams	Observations
316 Stainless	0.40	0.40	Light surface oxidation
316 Stainless	1.73	1.73	
321 Stainless	0.66	0.66	Heavy surface oxidation
347 Stainless	1.01	1.01	Light surface oxidation
410 Stainless	0.95	0.95	
430 Stainless	0.67	0.67	Heavy surface oxidation
Brass	0.42	0.38	
Monel	1.40	1.31	Medium surface oxidation
Teflon	0.44	0.44	No change
Buna rubber	0.27	0.17	Turned powdery
Nylon	0.12	0.06	Appeared dissolved
R.T.V. rubber	0.18	0.15	Surface reaction
Vitron rubber	0.14	0.16	Became pliable
Plex 55	3.78	4.78	Turned yellow and pliable
Sierracin 880	2.68	1.98	Turned yellow and slightly deformed

It should be pointed out here that the test conditions were very severe in comparison to the actual conditions that would exist in the cell during the sterilization test. Although the time and temperature are near those of the sterilization test the oxygen pressure and contamination by KOH would be much less.

The results show that the best type of stainless steel is either 316 or 347. Of course nickel is the most stable metal and could be used to protect other materials via nickel plating. Although all of the rubber materials would be unsuitable for such an environment they may still be employed for O-rings if very little or no KOH is present (see below). Since Teflon was found to be unaffected it should serve well as the bellows material. Although the Plex 55 intended for use as the spacer material was found to be badly deteriorated it may still be suitable for use within the cell covered by a layer of metals, the outermost of which is nickel, to protect the plastic from the KOH solution and oxygen. The thermal stability of Plex 55 appears suitable as a shrinkage of only 1.36 percent was observed on a sample held at 125°C for 30 hours while under compression equal to that within a cell. Plans are currently under way for corrosion tests on a sample nickel-plated spacer.

Another series of tests was carried out on the rubber materials eliminating the KOH solution. The object of these tests was to determine the extent of oxidation of rubber in pure oxygen. The tests were carried out at 125°C for sixty hours. One series was run at a relatively low oxygen pressure of 50 psig and one at a high pressure of 400 psig. The results were as follows:

P_{O_2} = 50 psig

Material	Initial Weight grams	Final Weight grams	Observations
Silicone	0.77	0.79	No change
RTV	0.50	0.49	Slight discoloration only
Neoprene	0.78	0.79	No change
Buna	0.26	0.25	No change

P_{O_2} = 400 psig

Material	Initial Weight	Final Weight	Observations
Silicone	0.63	0.66	Slight discoloration only
RTV	0.31	0.12	Decomposed
Neoprene	0.49	0.50	Deformed and hardened
Buna	0.26	0.28	Deformed and fused to wall

The results indicate that the stability of all the rubber samples is a very strong function of the oxygen pressure. At low pressures any of these would be suitable, but at high pressures only silicone rubber would be suitable.

4. PROTOTYPE DEVELOPMENT

The design and proposed testing of the first prototype are discussed in the following sections. Plans for the next prototype are also included.

4.1 Design Criteria

The design of the fuel cell portion of the first prototype (see Fig. 2) was based primarily on the first multicell unit developed on NASA Contract 7-7 (Ref. 1). There are no fundamental changes in the new unit, but several minor changes include the method of compressing the stack of cells and the number of gas manifolds. The compression in the new prototype is accomplished by a large bolt passing through the center of the cell stack rather than by several smaller bolts on the periphery of the cells. This change eliminated the problem of nonuniform compression caused by uneven tension on the several small bolts. As shown in Fig. 2, only one inlet hydrogen manifold was employed on this unit compared to both an inlet and exit manifold on the first model. The exit manifold, used only for flushing, was found to be unnecessary as the unit can now be flushed merely by purging. The only other changes in the fuel cell portion are in the electrode diameter (6 inches compared to 4 inches) and the number of cells (38 compared to 9).

The principal design criteria for the overall assembly were based on the elimination of the gas leakage problems. It was reasoned that if the fuel cell were to be located inside one of the gas storage chambers the pressure differential across the cell would be only a few pounds compared with 400 psi if not within the vessel, and the probability of gasleaks through the numerous (152) O-ring seals would be greatly reduced. Compactness was the second reason for the selection of the configuration.

The unit has been structurally designed to withstand the proposed operating pressures of 400 psi. The center bolt has been designed to support the fuel cell for the most severe environmental test of 200 g shock.

4.2 Fabrication and Testing

Fabrication of the component parts was begun in mid June and the unit should be ready for test in late July.

The objective of the first series of tests will be to establish the functionality of the fuel cell. To accomplish this test the unit will be run as a primary cell. The hydrogen end cap will be removed so that the cell stack is readily accessible and the gases will be supplied externally from H_2 and O_2 bottles. The unit will first be tested for leaks at 50 psi. If no leaks are found, the unit will be placed on discharge and voltage probes will be made on each cell. Voltage-current and voltage-time characteristics will be measured for each cell.

If the fuel cell is found to be functioning properly, the complete unit will be assembled and run as a secondary. The first test will consist of proof testing the pressure vessels at 600 psi with an inert gas. If successful, the unit will be cycled at various currents with the measurement of voltage, current, temperature, and pressure.

4.3 Future Prototypes

When satisfactory performance of the fuel cells on the first prototype is established (and no major problems are anticipated in establishing this point), the design of the fuel cell components of the assembly will be frozen. The fuel cells of all subsequent prototypes and those of the final units will be the same as the first except, perhaps, for a change in thickness of the cell spacers.

The preliminary heat transfer analysis of this first prototype (see Subsection 5.2) points out that one of the major problems will be transferring heat from the fuel cells to the environment. The analysis shows that present prototype configuration may have to be modified in order to improve the transfer of heat from the cells.

Any major changes to be encountered in future prototypes should not involve the fuel cell portion but rather the overall configuration of the fuel cell - gas storage chambers. The criteria for the best configuration will include considerations of heat transfer and reliability as well as weight, volume, and operating limits.

5. HEAT GENERATION AND TRANSFER

5.1 Heat Production in an Electrochemical Cell at Constant Volume

It can be shown that heat may be either produced or absorbed in an electrochemical cell when the cell is operating reversibly. The extent to which heat is either produced or absorbed in a real cell depends upon a number of factors, including inherent thermodynamic properties of the electrochemical system and the polarization characteristics of the cell. It is also dependent upon whether the cell is being charged or discharged, and whether the process occurs at constant pressure or constant volume. The present discussion concerns constant volume processes only, since rechargeable fuel cells will generally be operated in this manner.

5.1.1 Reversible Process

Since Q is generally defined as the heat input to a system and W the work output,

$$dU = dQ - dW_T \tag{1}$$

$$= dQ - (PdV + dW_{elec}) \tag{2}$$

where U is the internal energy, W_T is the total work output, and W_{elec} is the electrical work output. For the condition at constant volume

$$dA = -dW_{elec} \tag{3}$$

$$= dU - d(TS) \tag{4}$$

$$= dQ - dW_{elec} - TdS \tag{5}$$

$\therefore$,

$$- dQ = -TdS \tag{6}*$$

* This result also follows directly from the definition of entropy, but the present approach is helpful in evaluating the irreversible case.

In these equations A is the Helmholtz free energy and S is the entropy.

The instantaneous rate of heat production, by differentiating Eq. 6 with respect to time, is found to be

$$-\frac{dQ}{dt} = -\dot{Q} = -T\frac{dS}{dt} \tag{7}$$

Differentiating the relation

$$S = nS_m \tag{8}$$

yields

$$\frac{dS}{dt} = S_m\frac{dn}{dt} \tag{9}$$

where S_m is the molar entropy change and n is the number of moles.*

Then Eq. 7 can be expressed as

$$-\dot{Q} = -TS_m\frac{dn}{dt} \tag{10}$$

Equation 10 is general for any reversible electrochemical cell, but the primary interest in the present analysis concerns the hydrogen oxygen fuel cell. Since one mole of water per second (either produced or consumed) involves two Faradays per second, which in turn is 193,000 amps, it is seen that

$$\frac{dn}{dt} = \frac{i}{193,000} \tag{11}$$

where i is the electrical current in amps, and Eq. 10 can be put in the form

$$-\dot{Q} = -5.18 \times 10^{-6}\ i\ TS_m \tag{12}$$

The factor 193,000 has units of amp-sec/mole. This gives $-\dot{Q}$, the heat output power, in cals/sec when S_m has units of cals/deg/mole.

* S_m (in addition to H_m, which is introduced later) has a slight pressure dependence, but the effect is negligible.

5.1.2 Irreversible Process

On either charge or discharge a real cell will depart from reversibility to an extent expressed by its polarization. If there be defined a parameter, γ, so that

$$\gamma = \frac{E}{E^*} \tag{13}$$

where E is the operating potential for either charge or discharge and E* is the reversible potential, then Eq. 3 can be rewritten as

$$\gamma dA = -dW_{elec} \tag{14}$$

That this is true for either charge or discharge can be seen by examining Fig. 5, which represents the form of a typical charge-discharge polarization curve for a hydrogen oxygen fuel cell. The minimum charging potential for a given current density is given by E*, and it can be seen from the curve that a charging potential E_C is required to maintain a current density J_C, where $E_C > E^*$. During a given time interval the electric energy input, $-W_{elec}$, is no longer equal to ΔA (as it is for the reversible process) but is now equal to $\gamma\Delta A$, where $\gamma > 1$. Similarly, on discharge E* represents the maximum discharge potential while E_D is the cell potential while maintaining a current density J_D. The energy output in a given time interval is no longer given by $-\Delta A$ but is instead given by $-\gamma\Delta A$, where now $\gamma < 1$.

Three more points should be noted about the analysis thus far. First, γ is identical to the efficiency on discharge (where the efficiency is based on E^*) but is the efficiency reciprocal on charge. Second, it should be noted that ΔA, ΔH, and ΔS are all negative on discharge and positive on charge, and finally E* for a chemical reaction is temperature dependent. For the case of the reaction

$$H_2(g) + 1/2\ O_2(g) \longrightarrow H_2O(\ell) \tag{15}$$

Figure 6 gives the dependence of E* on the temperature where all species are in their standard states. E* under these conditions is equivalent to

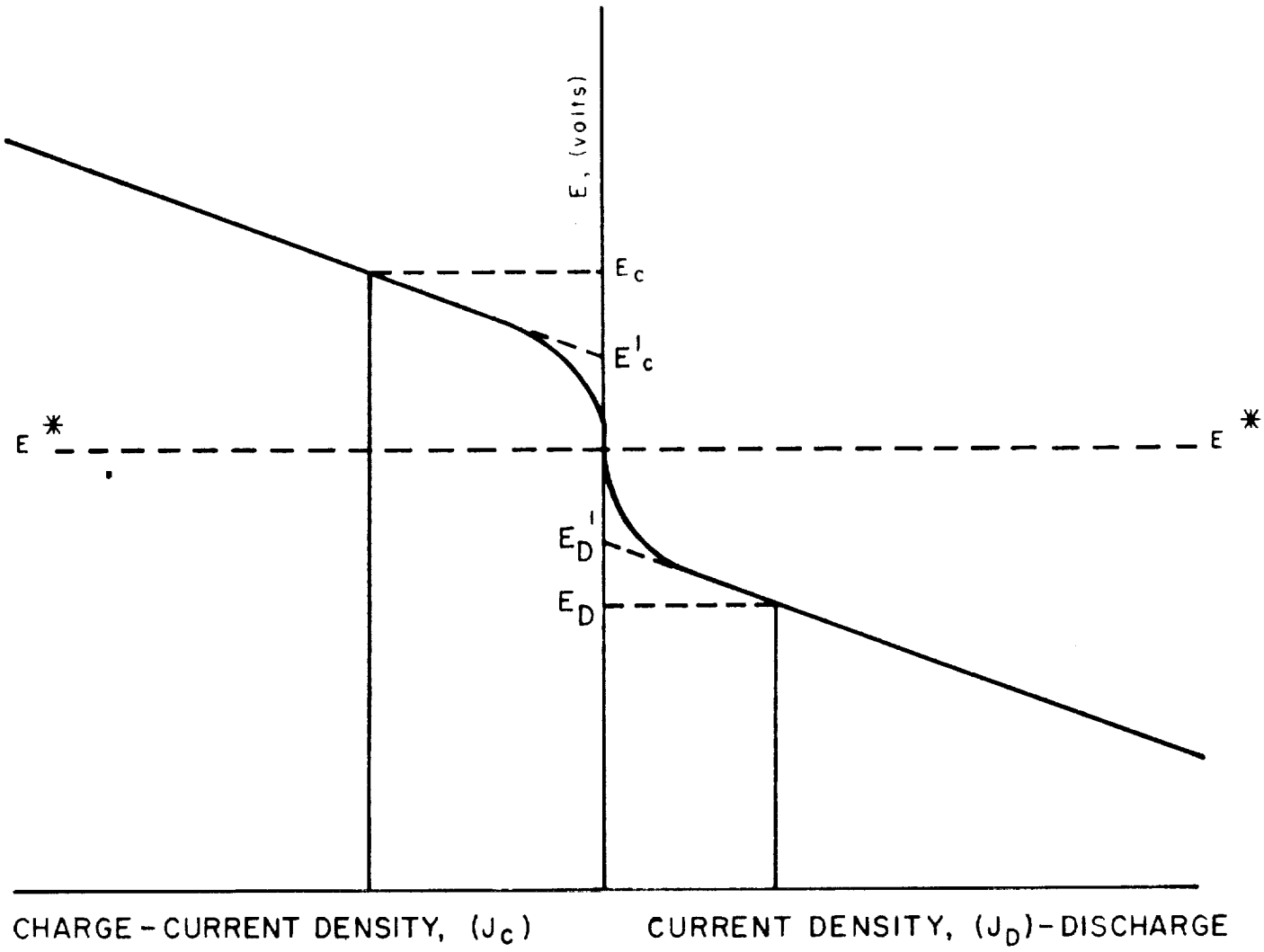

FIG. 5 HYPOTHETICAL CHARGE DISCHARGE POLARIZATION

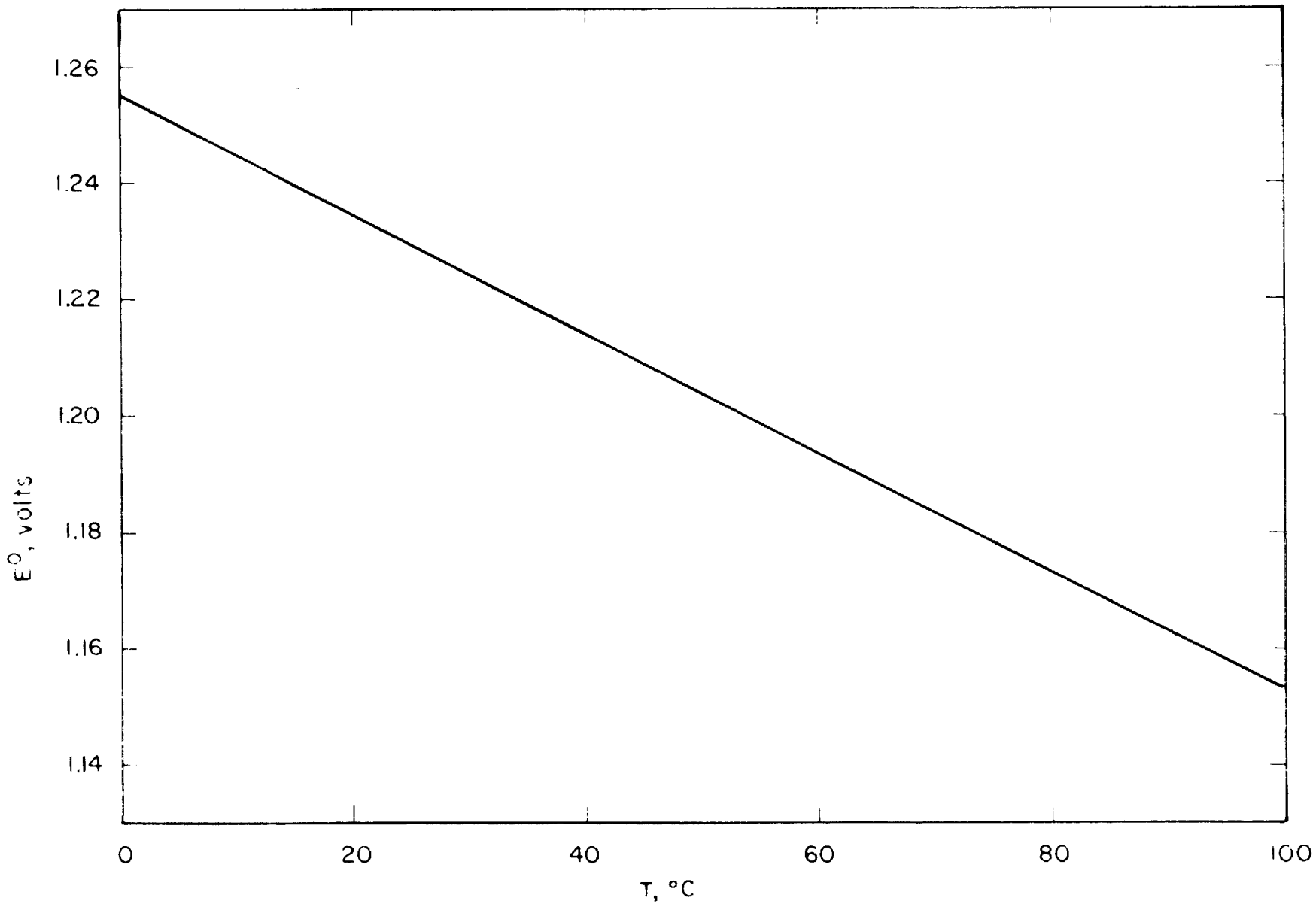

FIG. 6 STANDARD CELL POTENTIAL VS TEMPERATURE

E^{o}, the standard potential, but the E*'s for a real cell will deviate slightly from the curve since the operating pressures are often several atmospheres and because the activity of water in solutions of 35 percent KOH is somewhat less than unity. For these reasons hydrogen oxygen fuel cells can be operated at temperatures far in excess of the normal boiling point of water.

Substitution of Eq. 14 into Eq. 5 gives

$$dA = dQ + \gamma dA - TdS \tag{16}$$

$\therefore$,

$$-dQ = (\gamma-1)dA - TdS \tag{17}$$

$$= (\gamma-1)(dU - TdS) - TdS \tag{18}$$

$$= (\gamma-1)\, dU - \gamma TdS \tag{19}$$

$$= (\gamma-1)(dH - VdP) - \gamma TdS \tag{20}$$

The derivative with respect to time becomes

$$-\frac{dQ}{dt} = -\dot{Q} = (\gamma-1)\left(\frac{dH}{dt} - V\,\frac{dP}{dt}\right) - \gamma T\frac{dS}{dt} \tag{21}$$

Differentiating the relation

$$H = nH_m \tag{22}$$

yields

$$\frac{dH}{dt} = H_m\,\frac{dn}{dt} \tag{23}$$

where H_m is the molar entropy change. If ideal gas laws are assumed, then the relation

$$P = \frac{nRT}{V} \tag{24}$$

can be differentiated and it is seen that

$$\frac{dP}{dt} = \frac{RT}{V}\cdot\frac{dn}{dt} \tag{25}$$

Substitution of Eqs. 23, 25, and 9 into Eq. 21 yields

$$-\dot{Q} = \frac{dn}{dt}\left[(\gamma-1)(H_m - RT) - \gamma TS_m\right] \tag{26}$$

It can be seen that Eq. 26 reduces to Eq. 6 (the expression for the reversible case) as γ approaches unity.

An interesting conclusion drawn from Eq. 26 is that while $-\dot{Q}$ is always positive on discharge, it may be either positive or negative on charge, depending on the charging potential. The charging potential for which $-\dot{Q} = 0$ can be calculated from Eq. 26 and Fig. 5.

If $-\dot{Q} = 0$, then

$$\frac{dn}{dt}\left[(\gamma-1)(H_m - RT) - \gamma TS_m\right] = 0 \tag{27}$$

$\therefore$,

$$(\gamma-1)(H_m - RT) = \gamma TS_m \tag{28}$$

$$\gamma(H_m - RT - TS_m) = H_m - RT \tag{29}$$

and

$$\gamma = \frac{H_m - RT}{H_m - T(R + S_m)} \tag{30}$$

The value of γ at 25°C is calculated to be 1.206, and at 60°C it is 1.245, leading to values of E* of 1.483 volts and 1.495 volts, respectively.

Examination of Eq. 26 also shows that under most conditions of charge and discharge more heat will be generated on discharge than on charge. It might be desirable to operate a fuel cell at charge and discharge potentials such that heat production is the same for both cases. In an unchanging environment this would result in isothermal operation.

The necessary condition is

$$-\dot{Q}_C = \dot{Q}_D \tag{31}$$

Therefore,

$$\left(\frac{dn}{dt}\right)_C \left[(\gamma_C - 1)(H_{m,C} - RT) - \gamma_C TS_{m,C}\right]$$

$$= \left(\frac{dn}{dt}\right)_D \left[(\gamma_D - 1)(H_{m,D} - RT) - \gamma_D TS_{m,D}\right] \tag{32}$$

and since $H_{m,C} = -H_{m,D}$ and $S_{m,C} = -S_{m,D}$, the right-hand side of Eq. 32 can be written

$$\left(\frac{dn}{dt}\right)_D \left[(1 - \gamma_D)(H_{m,C} + RT) + \gamma_D TS_{m,C} \right]$$

Since the current density, J, is proportional to dn/dt, Eq. 32 can be rearranged and written as

$$\frac{J_C}{J_D} = \frac{(1-\gamma_D)(H + RT) + \gamma_D TS}{(\gamma_C - 1)(H - RT) - \gamma_C TS} \tag{33}$$

where H and S refer to $H_{m,C}$ and $S_{m,C}$ respectively. Equation 33 can also be written in the form

$$\frac{J_C}{J_D} = \frac{RT + H - \gamma_D (RT + H - TS)}{RT - H + \gamma_C (H - TS - RT)} \tag{34}$$

When numerical values are inserted for R, T, HH, and S, and the coefficient of γ_C is divided out, Eq. 34 becomes

$$\frac{J_C}{J_D} = \frac{1.265 - 1.024\ \gamma_D}{-1.242 + \gamma_C} \tag{35}$$

Therefore,

$$\gamma_C = 1.242 + \frac{J_D}{J_C} (1.265 - 1.024\ \gamma_D) \tag{36}$$

and since

$$J_D = \frac{E_D - E_D'}{\rho_C} \tag{37}$$

and

$$J_C = \frac{E_C' - E_C}{\rho_C} \tag{38}$$

where E_C' and E_D' refer to extrapolated open circuit potentials, Eq. 36 becomes

$$\gamma_C = 1.242 + \frac{E_D - E_D'}{E_C' - E_C} (1.265 - 1.024\ \gamma_D) \tag{39}$$

since it is assumed that the ρ's (the slopes of the polarization curves) are equal.

Values for the EOS fuel cell at 150° F can be taken as $E'_D = 0.93$ volt and $E'_C = 1.47$ volts. If on discharge $E_D = 0.80$ volt, then Eq. 39 becomes

$$\gamma_C = 1.242 + \frac{0.13}{1.47-E_C} \quad 1.265 - 1.024\left(\frac{0.80}{1.20}\right) = \frac{E_C}{1.20} \qquad (40)$$

Therefore,

$$E_C = 1.491 - \frac{0.0906}{1.47-E_C} \qquad (41)$$

Equation 41 is quadratic in E_C and when solved yields the values 1.78 volts and 1.18 volts. (The latter value clearly has no physical significance.) However, it may not be practical under some circumstances to charge at 1.78 volts and discharge at 0.80 volts as this leads to an efficiency of only 45 percent. When better electrodes are developed, however, isothermal operation at much higher efficiencies will be obtained at the same power levels.

The heat generated in a hydrogen oxygen fuel cell is shown in Fig. 7, where rate of heat output is plotted versus charging and discharging potentials. The shape of the curve, as well as the absolute magnitude of the rate of heat generation, is dependent upon the polarization curve for the cell. Figure 7 is based on the polarization curve of Fig. 8, which refers to the present EOS cell operating at 150° F. It should be born in mind that certain features of Fig. 7 are independent of the polarization curve. On discharge heat is always produced, while on charge heat is absorbed below a certain potential and produced above that point, and the potential at the crossover point is independent of the polarization curve. While it is theoretically true that heat is absorbed below a certain charging potential, the activation polarization at an oxygen electrode is generally so severe that current densities are infinitesimal in this region, and so, therefore, is the heat absorption.

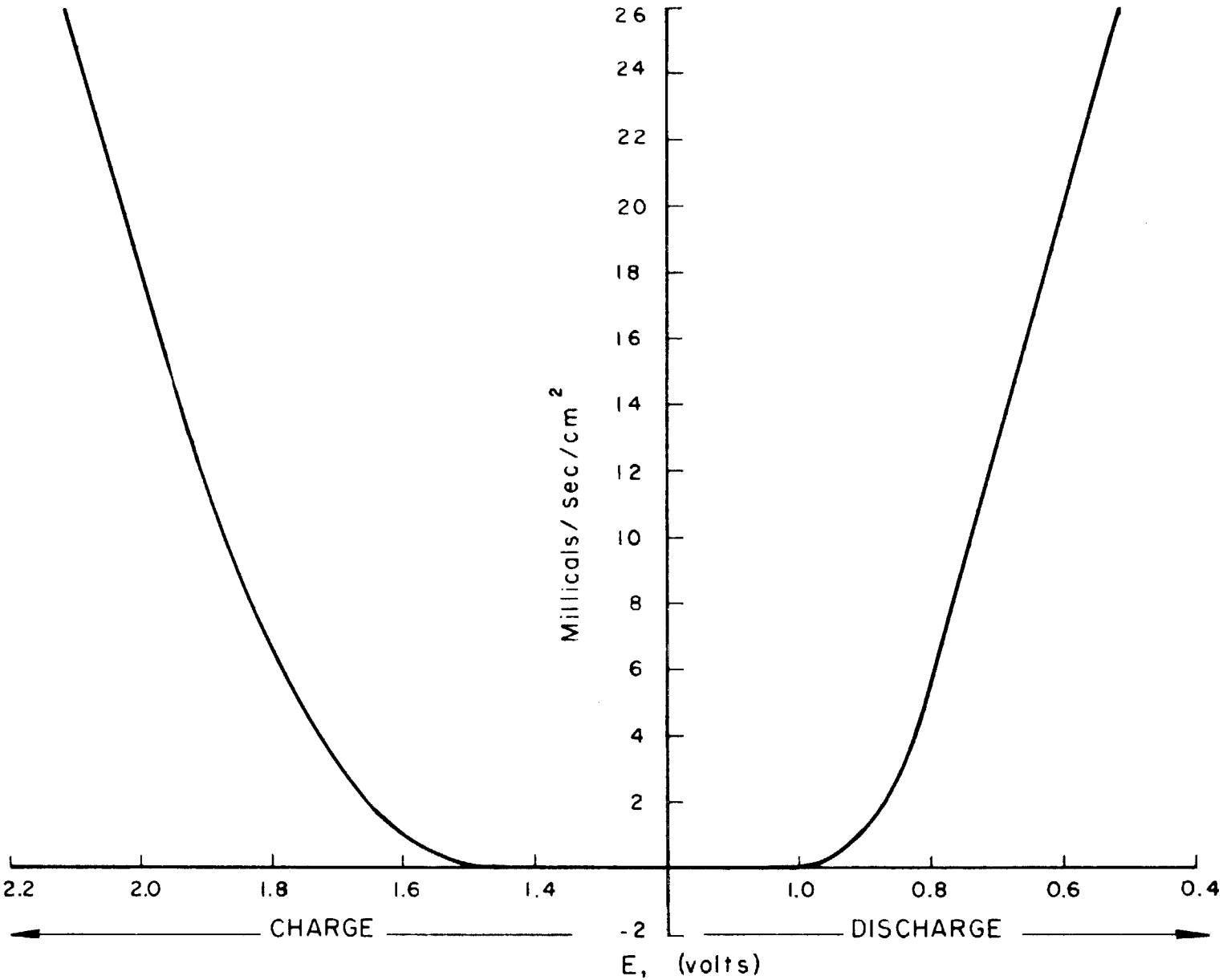

FIG. 7 HEAT GENERATION RATE VS CELL POTENTIAL

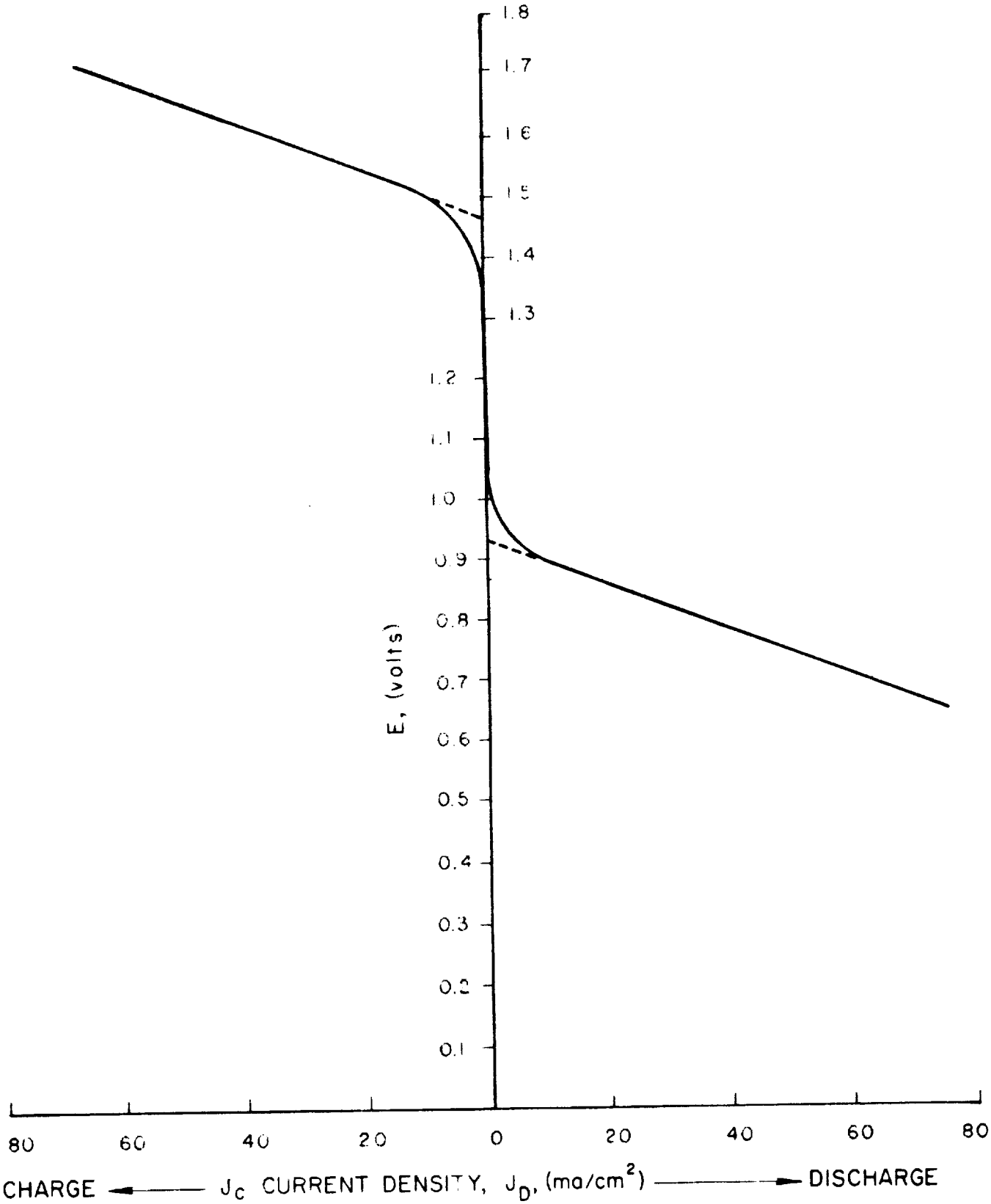

FIG. 8 POLARIZATION CURVE FOR EOS FUEL CELL AT 150°F

5.2 Heat Transfer

Preliminary heat transfer calculations have been made to identify problem areas. At the present time a more complete analysis is in progress to establish the trade offs (e.g. reliability, weight, volume, operating limits) associated with providing various solutions to the heat transfer problem. The preliminary heat transfer analysis of the first prototype is presented in the following subsections. The first section deals with the case of the unmodified design. The second section deals with the case where the design is modified so as to improve heat transfer.

The heat transfer paths within the assembly are given in the accompanying diagrams. Figure 9A gives the nomenclature. Figure 9B gives the heat flow path for the unmodified design in which the heat flows radially inward from the cells to a center tie bolt, across the bolt, to the base plate, and finally out the base plate to the gas cylinders. Figure 9C gives the path for the case where an aluminum sheath is tightly fitted to the cell assembly and receives the heat,which is transferred radially outward from the cells. Figure 9D gives the path for the case where the sheath is again employed and the position of the base plate is shifted to the center of the cell assembly.

5.2.1 Unmodified Design

One short calculation is sufficient to show that the unmodified design does not provide adequate heat transfer paths from the fuel cell to the gas cylinders. First let it be assumed that the only direction in which the heat may flow within the fuel cell is in a radial direction. (Axial flow is shown to be negligible in the next section.)

Next, examination of Fig. 9B indicates that the heat must flow from the fuel cell inward to the center tie bolt, and then through the tie bolt to the base plate. The temperature drop along

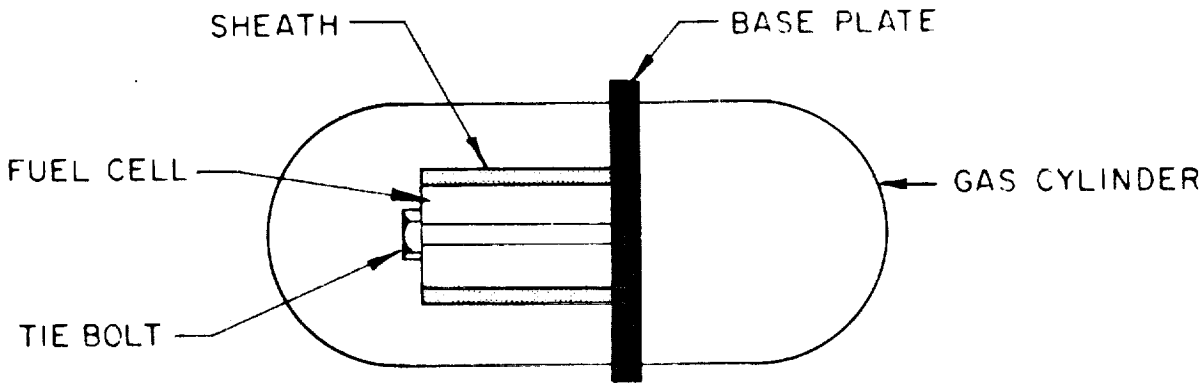

A. COMPONENTS OF ASSEMBLY

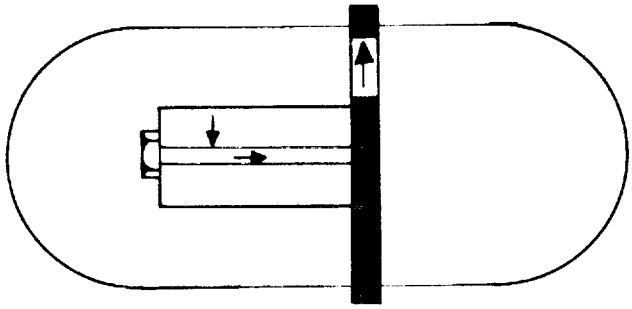

B. HEAT FLOW PATH FOR UNMODIFIED DESIGN

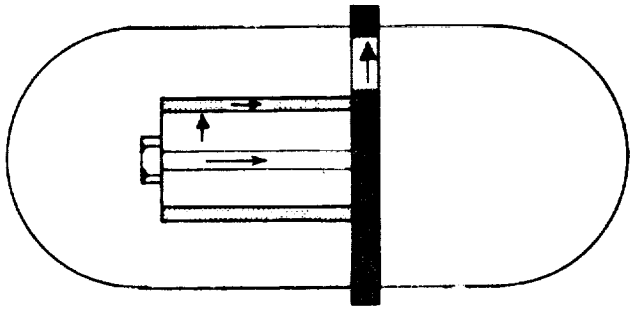

C. HEAT FLOW PATH WITH SHEATH

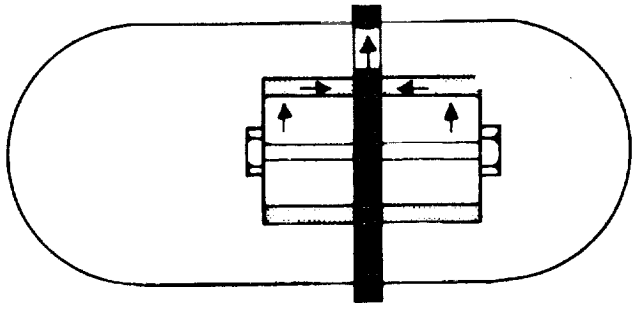

D. HEAT FLOW PATH WITH SHEATH AND DISPLACED BASE PLATE

FIG. 9 HEAT TRANSFER PATHS IN PROTOTYPE

the bolt may be estimated by the equation given by Hawkins (Ref. 2)

$$\Delta t = \frac{q''' L^2}{2\ k}$$

where

Δt = temperature drop ($^\circ$F)

q''' = volumetric heat generation rate (Btu/hr/ft^3)

L = length (ft)

k = thermal conductivity (Btu/(hr)(ft^2)($^\circ$F/ft))

For the given bolt length of 11 inches and diameter of 3/4 inch, and at the total heat load of 655 Btu/hr, the value of q''' is found to be 2.31×10^5 Btu/hr-ft^3. Employing a value of 9.0 Btu/(hr)(ft^2)($^\circ$F/ft) for k, the approximate conductivity of steel, the temperature drop across the bolt is found to be 10,700°F. This value for Δt is, of course, untolerably high as the maximum operating fuel cell temperature is 200°F. Even if the bolt were to be made of aluminum with a much higher conductivity of approximately 111(Btu/(hr)(ft^2) ($^\circ$F/ft), the value of Δt is reduced only to 890°F.

The above results indicate that additional heat transfer paths are mandatory in order to keep the fuel cell temperature below 200°F at the above heat load.

5.2.2 Modified Design

One possible modification of the original prototype design would be to enclose the fuel cell in a tightly fitted metal sheath as shown in Figs. 9C and 9D. This sheath would serve the purpose of lowering the extremely high temperature drop across the cells by providing a low resistance conduction path between the cells and the base plate. Conduction through the center bolt is neglected for this case.

The following subsections are concerned with an analysis of such a design. Radial heat transfer across the surface of the cells is discussed in subsection 5.2.2.1. Transfer across a thin insulating film inside the sheath is discussed in subsection 5.2.2.2. Transfer

along the sheath is discussed in 5.2.2.3 and radial transfer across the base plate is discussed in 5.2.2.4. Typical temperature drops along each component are presented in 5.2.2.5.

5.2.2.1 Radial Transfer in Fuel Cells

The fuel cell may be considered to consist of two concentric cylinders the inside diameter of which corresponds to the electrode diameter and the outside diameter of which corresponds to the outside edge of the cell spacers. Heat may be considered to be generated uniformly within the inside cylinder and transferred across the outside cylinder to the sheath.

For such a model the relationship between temperature and distance from the center is given by Hawkins (Ref. 2). From the o.d. of the inner cylinder to the axis:

$$t - t_1 = \frac{q'''}{4k} (r_o^2 - r^2)$$

where

t = temp at radius r, °C
t_1 = temp at o.d. of inner cylinder °C
q''' = volumetric heat generation rate cal/cm^3/sec
r_o = radius of inner cylinder cm
r = radius, cm
k = thermal conductivity cal/(sec)(cm^2)(°C/cm)

From the o.d. of the outer cylinder to the o.d. of the inner cylinder:

$$t_1 - t_2 = \frac{q'}{2\pi k} \ln \frac{r_2}{r_1}$$

where

t_1 = temp at o.d. of inner cylinder, °C
t_2 = temp at o.d. of outer cylinder, °C
q' = heat flow per unit length of cylinder cal/sec-cm
r_2 = radius of outer cylinder
r_1 = radius of inner cylinder
k = conductivity as above

Since the fuel cell is not homogenous but consists rather of alternate layers of metal, plastic, and electroyte, the value of the thermal conductivity in the above equations must be taken as a weighted average of the conductivities of the various materials. The following table lists the thicknesses "t", the thermal conductivities "k", and the product "t x k" for the various materials. Inspection of this table indicates that the product "t x k" for the plastic as well as for the electrolyte is negligible in comparison to that of the metal layers. Therefore, nearly all of the heat will flow radially outward through the metal layers with only a minute amount of axial flow across the cells.

THERMAL CONDUCTIVITY PROPERTIES OF FUEL CELL MATERIALS

Material	*t, Thickness (cm)	k, Thermal Conductivity, cal-sec, cm, $^{\circ}$c	t k x 10^4
Ni electrode	0.120	0.0045	5.4
Nickel	0.0150	0.140	21
Copper (1/2 mil)**	0.0026	0.92	24
Copper (1 mil)	0.0050	0.92	46
Copper (2 mils)	0.0100	0.92	92
Copper (3 mils)	0.0150	0.92	138
Silver	0.0050	0.99	50
Plastic	0.515	0.0005	2.5
Electrolyte	0.09	0.0012	1.1

* For a complete cell there are two electrodes and two layers of each metal coating on either side of the spacer. Therefore the values of thickness in this column are for two layers of each material.

** The thickness of the copper layer is taken as a parameter.

The heat generation rate is taken as 192 watts (655 Btu/hr). With this value and the above equations for the given cell dimensions, the radial temperature profiles were calculated for assumed variations in the thickness of the electroplated copper layer (heat

transfer through the plastic and electrolyte were disregarded and cell spacers were assumed to be coated with 1 mil of silver and 3 mils of nickel).

The results of these calculations are shown in Fig. 10. Inspection of this figure reveals that the temperature difference between the axis and the outside edge of the fuel cell will be approximately 6° to 13°C depending of course on the thickness of the copper layer.

5.2.2.2 Transfer Across Insulating Film

The sheath must be electrically insulated from the cells in order to avoid short circuits. For the purpose of this analysis it will be assumed that the sheath will be lined on its inside with a thin film of Teflon. The temperature drop across this film is calculated by the basic conduction equation, i.e.,

$$\Delta t = \frac{Q\ell}{kA}$$

where

Δt = temperature drop (°F)

Q = total heat load (Btu/hr)

ℓ = thickness of film (inches)

k = thermal conductivity of Teflon (Btu/(hr)(ft^2))(°F/in))

A = area (ft^2)

By substitution of the known heat load of 655 Btu/hr, an area of 1.68 ft^2, and thermal conductivity of 1.45 for Teflon in the above equation, the relation between the temperature drop across the film and thickness is given by the following:

$$\Delta t = 270\ell$$

The linear relation is shown in Fig. 11.

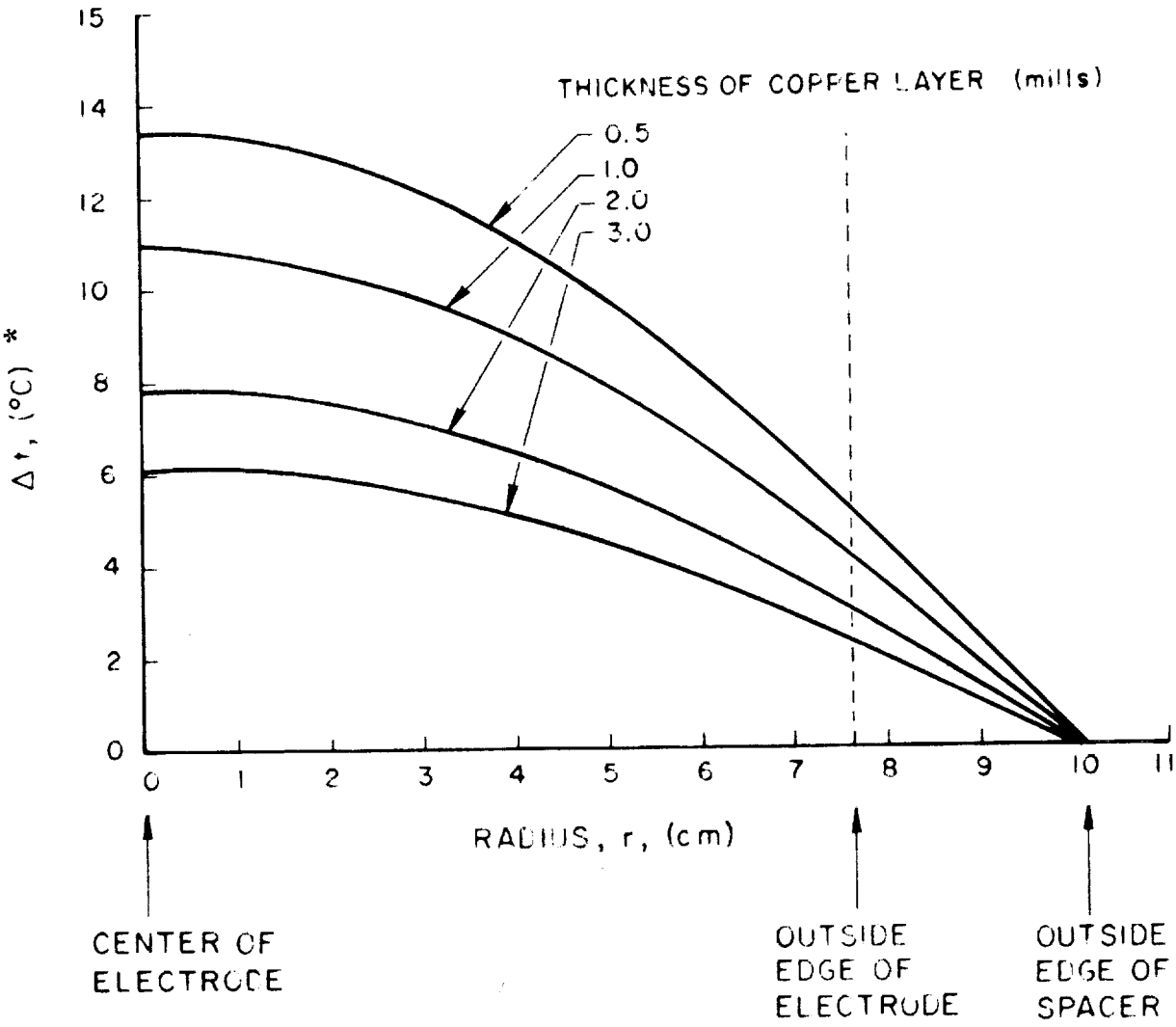

FIG. 10 RADIAL TEMPERATURE DROP IN FUEL CELL

* Δt is the difference in temperature between a point at radius "r" and the outside edge of the spacer.

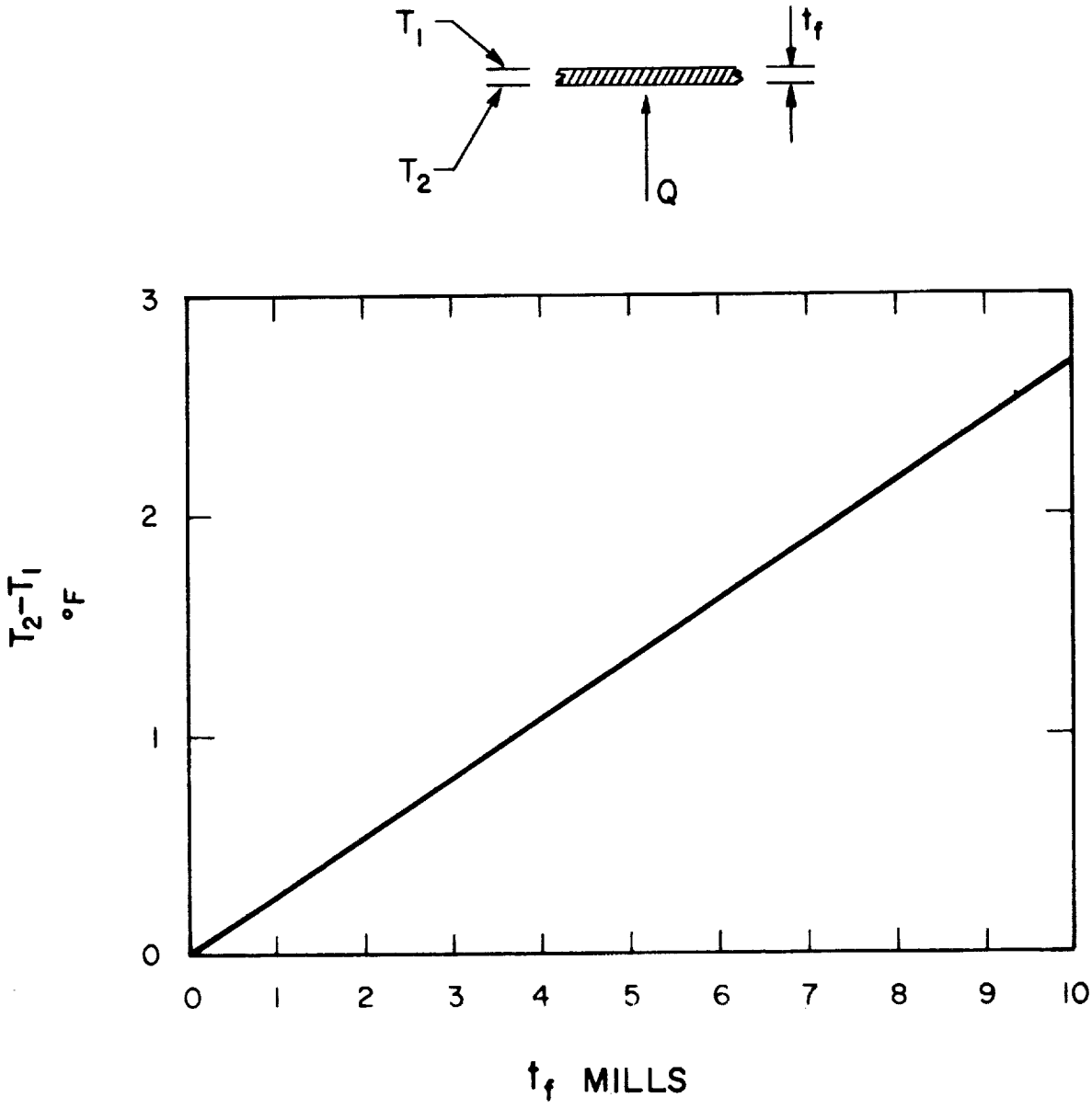

FIG. 11 TEMPERATURE DROP ACROSS TEFLON INSULATOR

5.2.2.3 Sheath Heat Transfer

After the heat has been transferred through the insulating film it will be transmitted to an aluminum sheath that surrounds the cell assembly over its entire length and makes solid thermal contact with the base mounting plate. Two types of temperature drop will be considered. The first is based on the existing cell assembly design in which the single mounting plate is attached to one end of the cell assembly. The second case will be for the mounting plate attached at the center of the cell assembly. As is subsequently noted for the equivalent thickness of the aluminum sheath, the temperature drop to the center mounted base plate compared to the temperature drop at the end mounted base plate varies by a factor of 4. Two curves are appended: the first or the end mounted plate showing the temperature differential using both aluminum or copper vs. sheath thickness (Fig. 12); the second curve uses the same parameters for the center-mounted plate (Fig. 13).

The basic equation used for determining temperature drop has been extracted from Hawkins (Ref. 3) and is for the case of a constant heat source across a flat plate. It is reasonable to assume that this equation sufficiently approximates the case of interest here since 38 uniform equal heat sources exist across an eleven-inch length.

The analysis is given below.

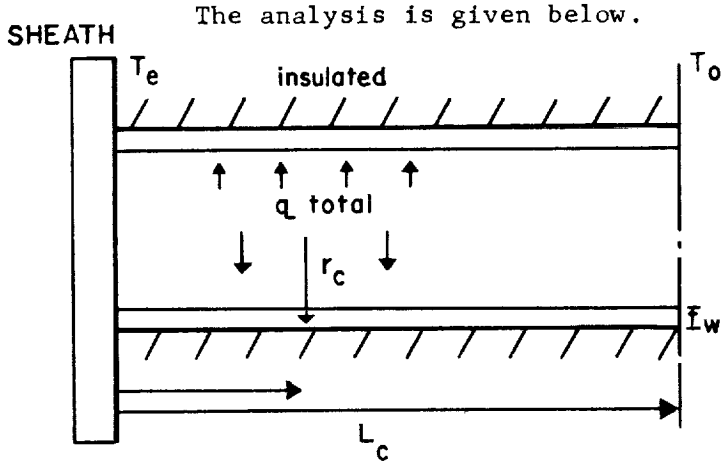

For constant thickness t_w:

$$T_o - T_e = q''' L_c^2/2k$$

$$= q_{total} L_c^2/2k \; 2\pi r_c t_w L_c$$

$$= \frac{q_{total} L_c}{4\pi k r_c t_w}$$

For the case of interest

$$q_{total} = 655 \text{ Btu/hr}$$

$$L_c = 11" = 0.916 \text{ ft}'$$

$$k_a = 100 \text{ Btu/hr ft } ^\circ\text{F (Aluminum Alloy)}$$

$$k_c = 220 \text{ Btu/hr ft } ^\circ\text{F (Copper)}$$

$$r_c = 7+2" = 0.292 \text{ ft}$$

and

$$(T_o - T_e)_{Al} = \frac{(655)\ (0.916}{(4)(3.14)(100)(0.292)} \frac{1}{t_w} = \frac{1.635}{t_w}$$

for t_w in inches $= 19.6/t_w$

$(T_o - T_e)_{Cu} = 8.9/t_w$

If the support is in the middle, then:

$$L_c = 0.458 \text{ ft}$$

$$g_t = 328 \text{ BTU/hr}$$

and

$$(T_o - T_e)_{Al} \simeq 4.90/t_w$$

$$(T_o - T_e)_{Cu} \simeq 2.22/t_w$$

With the above equations, the temperature drops along the sheath were calculated for various assumed thicknesses of the sheath. The resultant curves for both end- and center-mounted base plates are shown in Figs. 11 and 12. Two curves are shown; one for the case in which the plate is made of aluminum, and one for copper.

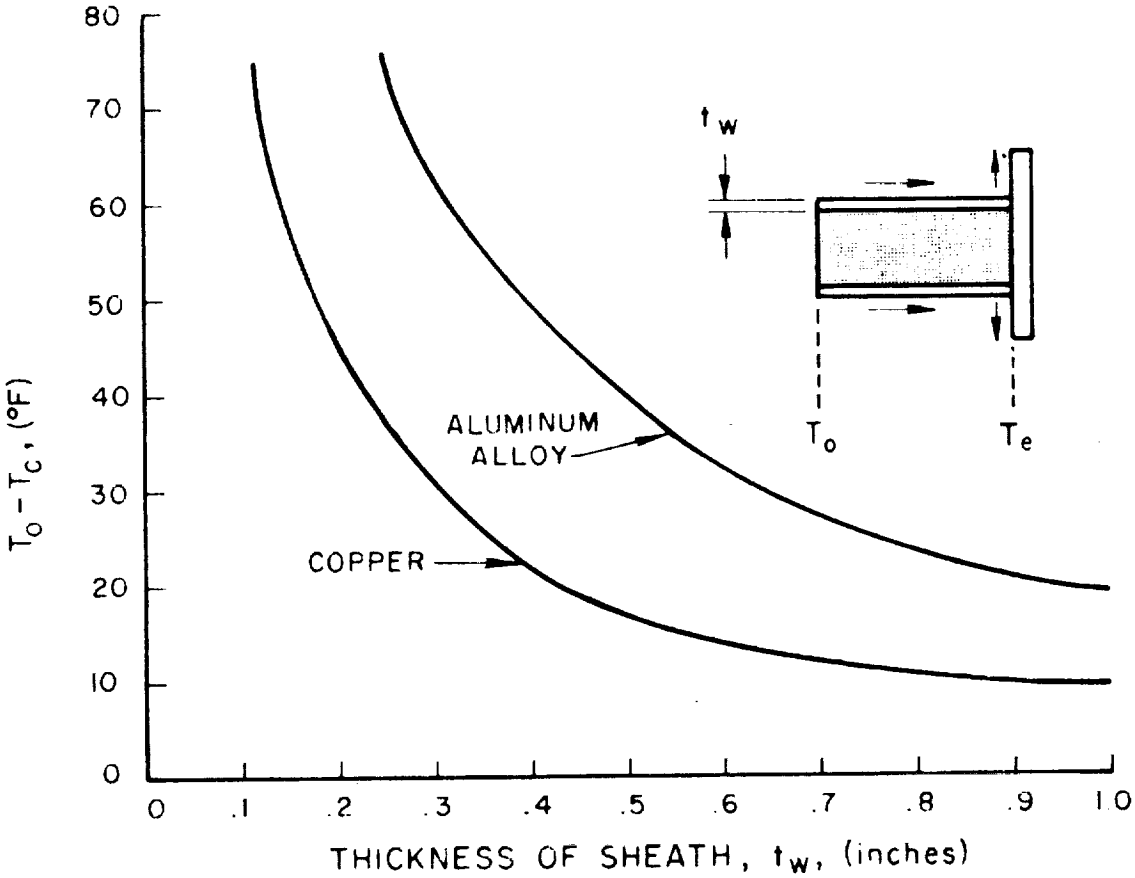

FIG. 12 TEMPERATURE DROP ALONG SHEATH WITH END MOUNTED BASE PLATE

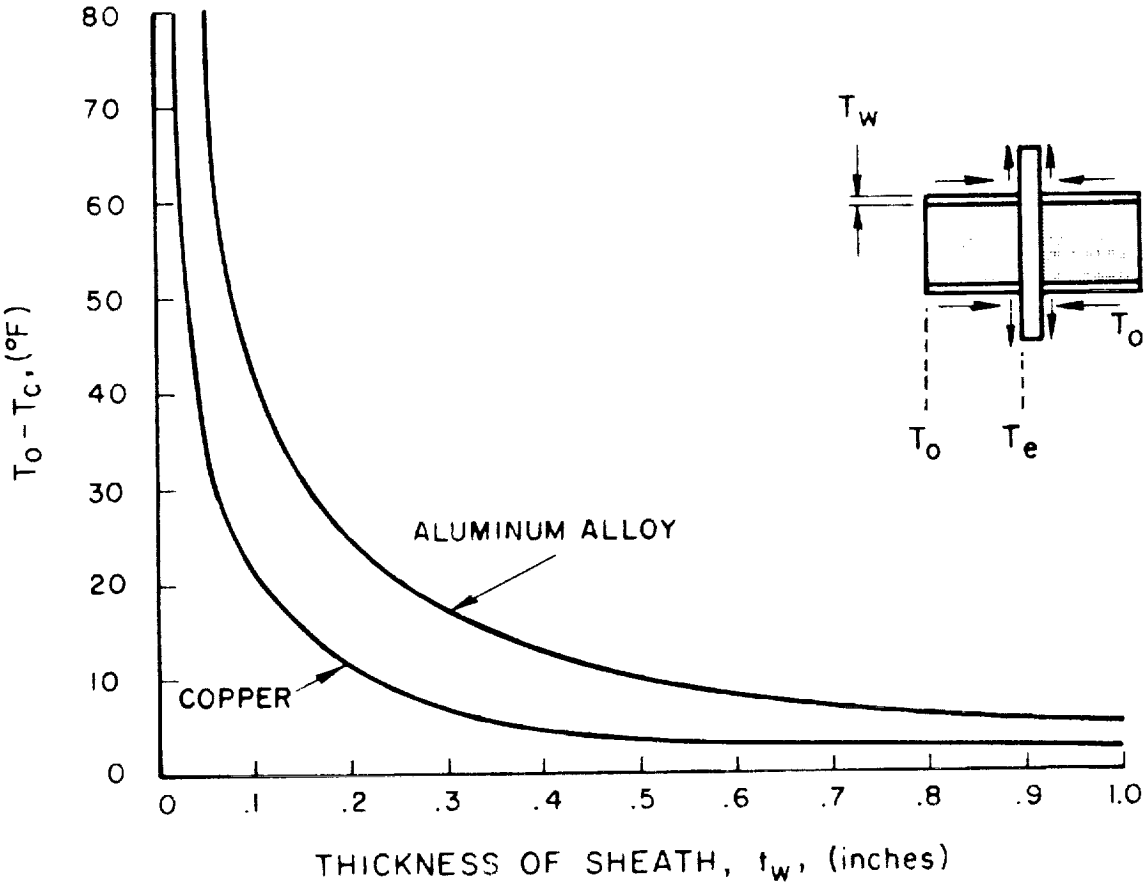

FIG. 13 TEMPERATURE DROP ALONG SHEATH WITH CENTER MOUNTED BASE PLATE

The number of base plates, although not considered in this analysis, is also a very important parameter. For example, if the cell stock were broken into three equal sections and two base plates were employed between the first and third sections then it can be shown that the temperature drop across each section of sheath would be only 1/9th of that which would exist across the single long sheath with only one end-mounted base plate.

5.2.2.4 Base Plate Heat Transfer

The temperature drop across the base plate is the same for the case of both the end and center mounting. This is due to the obvious fact that the total amount of heat transfer is independent of the base plate location. The following calculations assume that all energy is transferred to the base plate in a circumferential area 7 inches in diameter. The base plate temperature drop curves are based on radial heat transfer to a 12-inch diameter. For purposes of these calculations, it is assumed that the disc is isothermal in the axial direction.

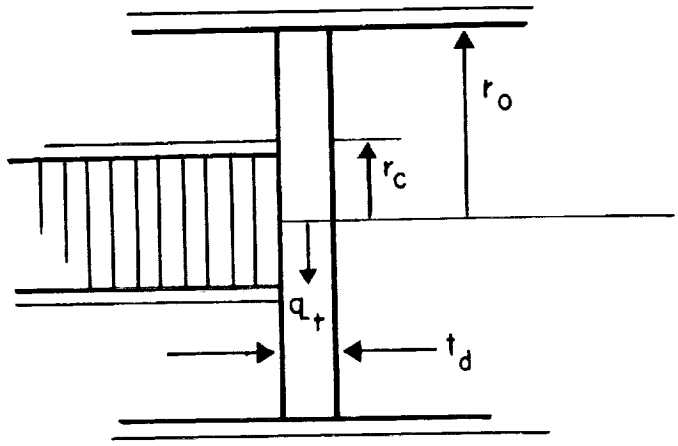

The equation describing heat transfer is given by Hawkins (Ref. 4):

$$T_c - T_o = \frac{q_t}{t_d} \frac{1}{2\pi k} \ell n \frac{r_o}{r_c}$$

For the case of interest $q_t = 655$ Btu/hr-ft$^{\circ}$F

$k_a = 100$ Btu/(hr - ft^2)($^{\circ}$F/ft) aluminum alloy

$k_c = 220$ Btu/(hr - ft^2)($^{\circ}$F/ft) copper

$r_o = 6"$

$r_c = 3.5"$

t_d = thickness of disc, ft

$$\ell n \frac{r_o}{r_c} = \ell n\ 1.715 = 0.54$$

For aluminum

$$T_c - T_o = \frac{655\ (.54)}{(6.28)(100)} \quad \frac{1}{t_d} = \frac{.563}{t_d}$$

For t_d in inches

$$T_c - T_o = \frac{6.77}{t_d}$$

For copper

$$T_c - T_o = \frac{3.07}{t_d}$$

With the above equations, the radial temperature drops across the base plate were calculated for various assumed values of the thickness of the plate. Two curves are shown: one for the case in which the plate is made of aluminum, and one for copper. (See Fig. 14.)

5.2.2.5 Combined Temperature Drop

The total temperature drop from the center of the end fuel cell to the gas cylinder may now be calculated for assumed values of the parameters in the above equation.

For an end mounted base plate of 1/2-inch aluminum, a sheath of 1/2-inch aluminum, with 3 mils of Teflon insulation and an electroplated layer on the plastic spacer consisting of 3 mils of nickel, 3 mils of copper, and 1 mil of silver, and at a total heat load of 655 Btu/hr, the following Δt's are found:

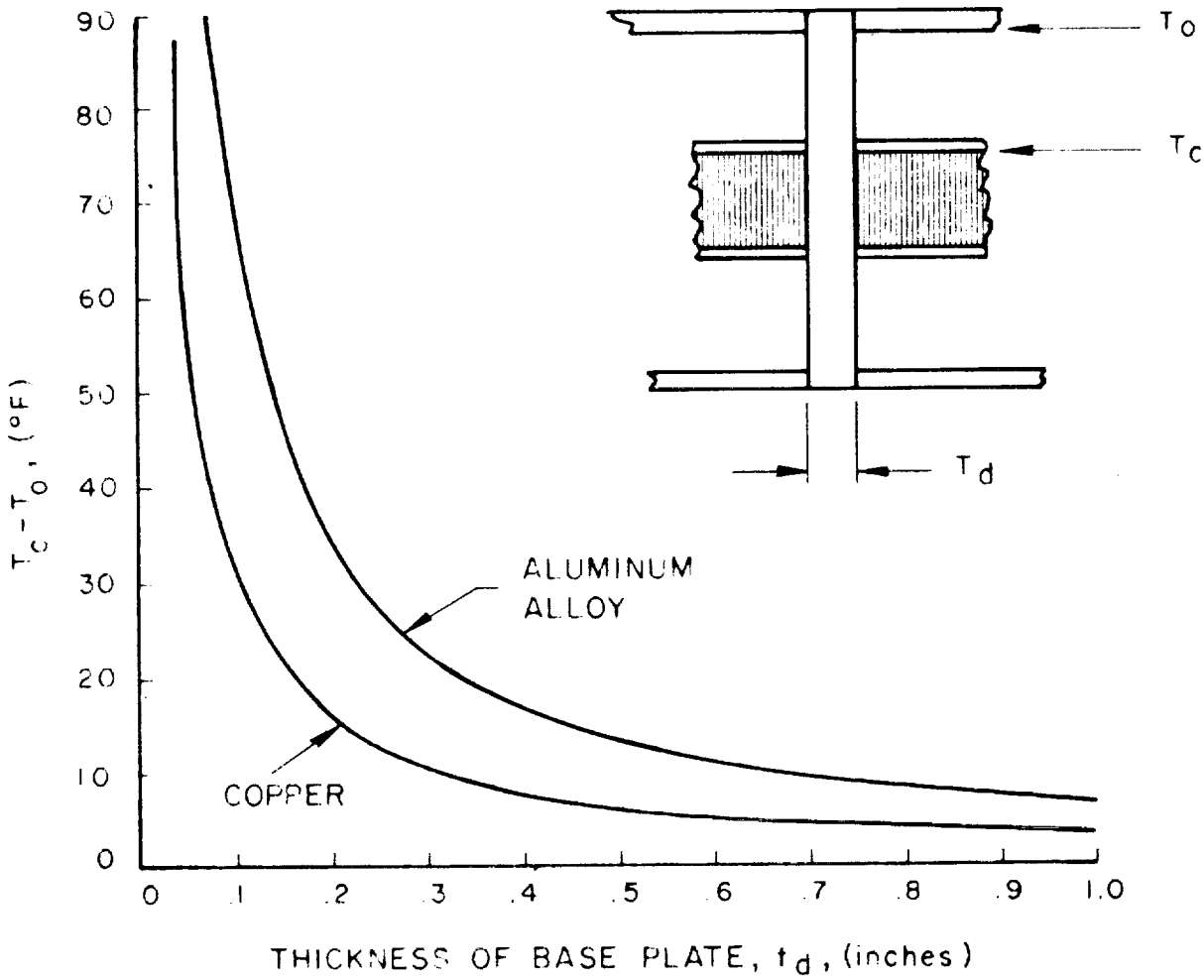

FIG. 14 RADIAL TEMPERATURE DROP ACROSS BASE PLATE

Δt from centerline of cells to o.d. of spacer	$10.8^{\circ}F$
Δt across 1/2 mil Teflon insulator	$0.8^{\circ}F$
Δt across sheath	$39.2^{\circ}F$
Δt across base plate	$13.5^{\circ}F$
Δt total	$64.3^{\circ}F$

Calculations are currently being made to determine the cylinder surface temperatures required for radiation of various assumed heat loads. For the above heat load of 655 Btu/hr the required temperature is near $120^{\circ}F$. The internal fuel cell temperature is determined by addition of the combined temperature drop to the cylinder surface temperature. For the above case the internal fuel cell temperature is thus found to be near $185^{\circ}F$.

These results signify that the incorporation of an aluminum sheath and base plate into the design of the first prototype would permit reasonable operating fuel cell temperatures (less than $200^{\circ}F$) for continuous operation at high load. The use of additional base plates or operation at lower loads would give lower fuel cell temperatures than in the above case (calculations are currently being made to determine the internal cell temperature as a function of the number of base plates and the heat load).

Although there are advantages for the use of a sheath and additional base plates from a heat transfer point of view, there are disadvantages from a mechanical point of view, i.e., gas sealing and assembly problems, and increased weight. Consequently, consideration is being given to alternative fuel cell-gas cylinder configurations. Calculations are being made to establish trade-offs as regards performance, reliability, weight and operating limits.

6. QUALITY CONTROL

To insure identical performance characteristics of the cells, all raw materials and fabrication techniques must be controlled. Tentative specifications for raw materials and processing details have been established and are for raw materials and processing details have been established and are given in the following subsections. All tests except those on the nickel plates and asbestos are performed at EOS. The supplier of these materials will certify the listed specifications:

6.1 Specifications

The following are tentative test specifications:

ITEM		INSPECTION	SPECIFICATION
Distilled water		Resistivity	$> 10^5$ ohm/cm^3
KOH solution		Concentration	35 $\pm$ 2%
Acid copper bath	a.	Concentration	32 $\pm$ 2 oz/gal
	b.	pH	0.70 $\pm$ 0.5
Silver cyanide bath	a.	Concentration	3.0 $\pm$ 0.1 oz/gal
	b.	pH	1.1 $\pm$ 0.5
Nickel sulfamate	a.	Concentration	64 $\pm$ 3 oz/gal
	b.	pH	4.5 $\pm$ 0.2
Platinum chloride solution	a.	Concentration	126 $\pm$ 2 gm/cc
	b.	pH	2.00 $\pm$ 0.01
Porous nickel	a.	Thickness	0.022 $\pm$ 0.002 inches
	b.	Weight	0.72 $\pm$ 0.16 gms/in^2
	c.	Porosity	80 $\pm$ 6%
	d.	Iron	< 0.02%
	e.	Sulfur	< 0.001%
	f.	Carbon	< 0.20%
	g.	Cobalt	< 0.001%

ITEM	INSPECTION	SPECIFICATION
Asbestos	a. Thickness	0.033 ± 0.003 inches
	b. Weight	0.53 ± 0.02 gms/in^2
	c. Asbestos	> 95%
	d. Organic	< 3%
	e. Ignition loss	< 18%
O-rings	a. o.d.	± .03%
	b. Thickness	± 2.5%
Fittings and valves	a. Visual	No scratches
	b. Leak test	No leaks at 400 psig
Pressure gages	a. Calibration	± 0.5%
	b. Leak test	No leaks at 400 psig
Cell spacers	a. Depth of O-ring grooves	0.081 ± 0.001 inch
	b. Manifold diameter	0.062 ± 0.005 inches
	c. Depth of electrode recess area	0.022 ± 0.001 inches
Electrolyte bed	a. Dry wt.	0.53 ± 0.02 gms/in^2
	b. Wet wt.	0.98 ± 0.05 gms/in^2
Platinized electrode	Activity	0.80 ± 0.06 volts at 15 ma/cm^2

6.2 Test Procedures

6.2.1 Resistivity of Distilled Water

The resistivity of the distilled water is measured by a conductivity bridge that is an integral part of the model B.D.-5 Bantam demineralizer unit. Alternatively, a sample may be taken, inserted in a conductivity cell with known cell constant, the resistance measured, and the resistivity calculated.

6.2.2 KOH Concentration

The potassium hydroxide solution is measured by taking a sample, adding phenolphthalein indicator, and titrating with a standard acid solution.

6.2.3 pH

The pH of all solutions is measured with a Beckman "Zeromatic" pH meter.

6.2.4 Platinum Chloride Content

The platinum chloride content of the plating solutions is measured by a conductivity test. The sample is placed in a conductivity cell, with known cell constant, and the conductivity is measured at a given temperature and pH. The platinum chloride content is then read from a calibration curve relating conductivity to concentration. This calibration curve was determined at constant temperature and pH by measuring the conductivities of solutions of known platinum chloride content.

6.2.5 Leak Testing

Two types of leak tests are employed on any component fitting or assembly. The first test consists of pressurizing the part to 400 psig and applying a soap solution. If no visual leaks are found, as indicated by the absence of bubbles, the part is connected to a small vessel, pressurized to 400 psig and then let stand for 24 hours. The presence of leaks is noted by a decline of pressure.

6.2.6 The dimensions of all components with specified tolerances are measured with conventional devices such as calipers and micrometers.

6.2.7 Conductivity of Plating on Spacers

The conductivity of the metal coating on the plastic spacers is measured in a specially designed apparatus as shown in Fig. 15. The spacer is placed on the pedestal that contains two poses with knurled surfaces for good electrical contact. A 50-lb weight is then placed on top of the assembly and the electrical resistance is read with an impedance bridge.

6.2.8 Activity of Electrodes

A 1 5/8-inch diameter sample is cut from the electrode and employed as the oxygen electrode in a cell with another 1 5/8-inch

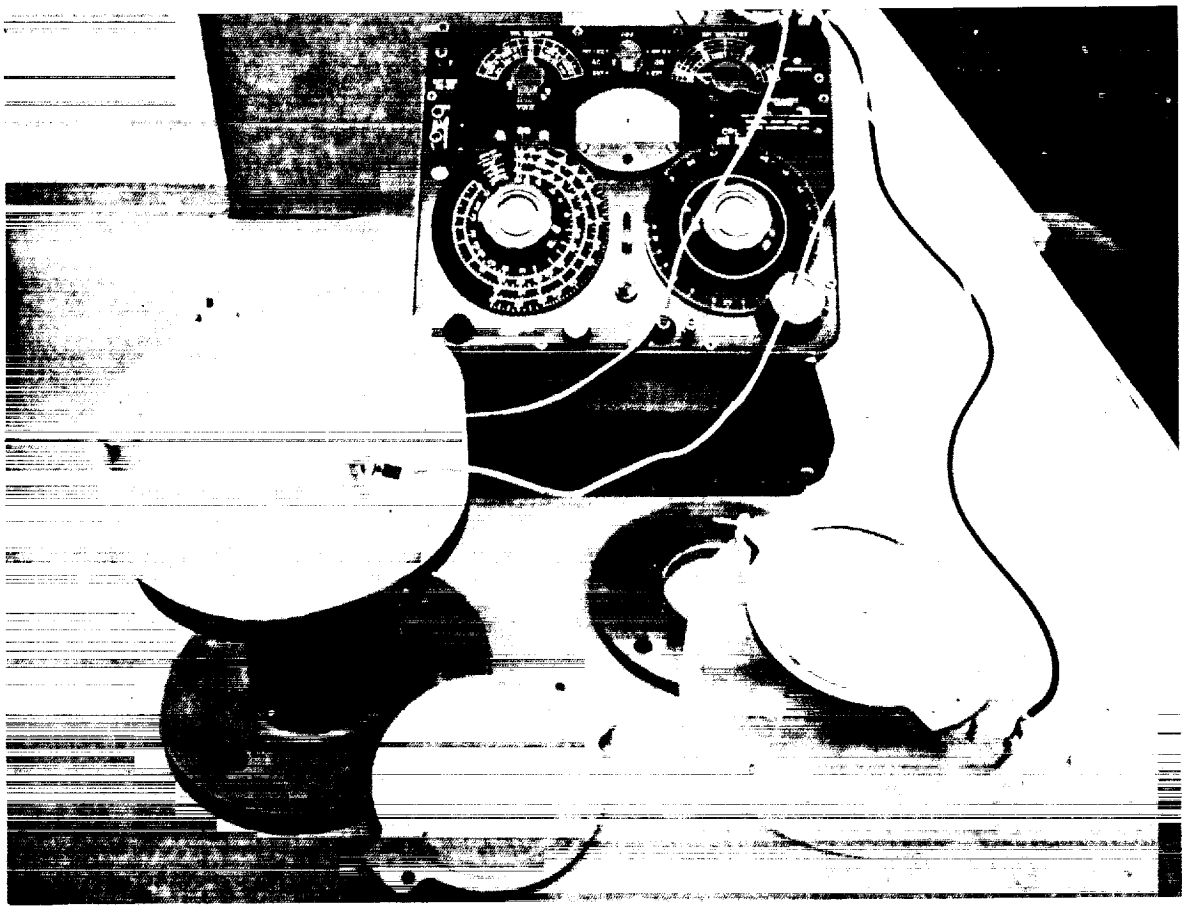

FIG. 15 APPARATUS FOR MEASUREMENT OF THE CONDUCTANCE OF THE PLATED SPACERS

diameter hydrogen electrode. The cell is then run at 50 psig gas pressure, supplied from externally located H_2 and O_2 cylinders, and at room temperature. The discharge voltages are measured at currents of 25, 50, 100, 200, 300, and 500 ma. The resultant V/I curve is a measure of the electrode activity. The discharge voltage at 15 ma/cm^2 for an active electrode has been arbitrarily set as 0.80 volts. The deviation from this voltage at the given current density describes the activity.

6.3 Processing Procedures

The following procedures are employed in the preparation of the fuel cell components.

6.3.1 Electrolyte Bed Preparation

The asbestos disc is cut by a die, weighed with an analytical balance, and then saturated with potassium hydroxide solution contained in a plastic squeeze bottle. The excess solution is removed by blotting with several layers of filter paper and the blotting process repeated until the disc contains the proper amount of electrolyte.

6.3.2 Spacer Plating Procedure

1. The surface of the Plexiglass 55 spacer is roughened by sandblasting to enhance the adherence of the silver plate.
2. To remove any oil and grease the spacer is washed in a detergent and rinsed with water.
3. The spacer surface is sensitized by application of a 0.1 N solution stannous chloride and then rinsed with water.
4. A mirror silver layer is sprayed on the spacer's surface with care so that all recesses are covered with silver. The product used is a commercial silver spray solution from the L.H. Butcher Company.
5. The silver coated spacer is placed in a copper hanger where it remains for the rest of the treatment. The hanger permits a more even deposition of metal on the spacer; however, it does draw a small amount of current away from the edges of the spacer. The spacer is attached to the hanger by small copper wires.

6. A copper strike about 0.0005 inch is applied at 18 amps/ft^2 for 20 minutes using an acid copper sulfate bath at a concentration of 32 ounces/gallon with pH at 0.7 and temperature at 70°F.
7. The spacer is rinsed with water and immersed into a 10 percent solution of NaCN to acclimate it to a cyanide environment.
8. The spacer is then transferred to a tank containing a potassium silver cyanide solution of 3 ounces per gallon at a pH of 11.0 and a temperature of 70°F. The silver plating process is carried out for 60 minutes at 6.2 amps/ft which gives a 1 mil layer of silver.
9. The spacer is removed from the tank, rinsed thoroughly with water, and immersed in a 40 percent H_2SO_4 solution.
10. The spacer is rinsed with water and then immersed in a nickel sulfamate bath of 64 ounces per gallon with pH at 4.5 and temperature at 100°F. A 10 amp/ft^2 nickel plate is applied for 3 hours. The final thickness of nickel plate should be 1/2 to 3/4 mil in the grooves and at least 3 mils on the outer edges.

6.3.3 Electrode Plating Procedure

CAUTION

Use plastic gloves at all times whenever handling the electrodes.

1. Prepare a solution of chloroplatanic acid such that 10 cc of this solution contains enough platinum to cover a surface with 40 mg per square inch of platinum black.
2. Insert a glass plating vessel into a constant temperature circulating bath.
3. Heat this bath to an equilibrium temperature of 82°C.

4. Add to the plating vessel a solution composed of 10 cc of chloroplatanic acid solution diluted to an amount sufficient to cover the electrode to be treated (400 cc).
5. Insert the nickel electrode between the arms of the stirrer propeller as shown in Fig. 16.
6. Allow plating solution to come to 75°C and then insert the electrode and the propeller into the plating solution.
7. Continue plating with agitation for 15 minutes at which time the solution should be a greyish-green color.
8. Remove stirrer and platinized nickel electrode from the vessel, separate the electrode from the stirrer propeller, and wash the electrode several times in distilled water.

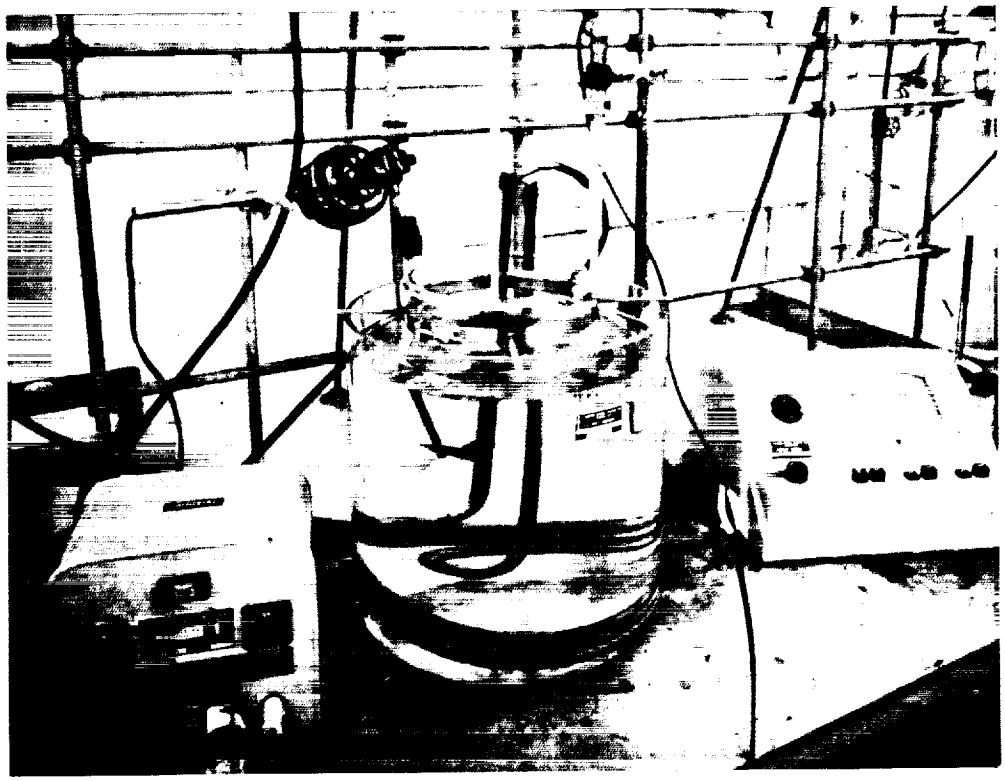

FIG. 16 APPARATUS FOR PREPARATION OF THE PLATINIZED NICKEL ELECTRODES

7. CONCLUSIONS

7.1 Fuel Cell

No major problems should be encountered in making the fuel cell portion functional in the first prototype. Important dimensions and processing techniques have been established. Some variation in the performance of cells within a stack is to be expected, but the degree of variation can be reduced by closer quality control. Pure nickel is the best metal and silicon rubber is the best rubber material for the corrosive environment within the cell.

7.2 Heat Generation

The heat generation within a fuel cell can be expressed in terms of the thermodynamics of the chemical reaction and the voltage-current characteristics of the unit cell.

7.3 Heat Transfer

The most important problem area is that of heat transfer from the fuel cell to the environment. Modification or redesign of the fuel cell - gas cylinder configuration of the first prototype will be necessary for continuous operation at high power levels.

7.4 Safety

Mixtures of hydrogen and oxygen at 100 psig and room temperature do not react explosively in the presence of the platinized nickel-KOH-asbestos assembly.

8. PLANS FOR SECOND QUARTER

8.1 Test First Prototype

Fabrication of the first prototype will be completed and testing begun. The object of the first test series will be to establish the functionality of the fuel cell portion of the assembly. Voltage-current, voltage-time, and leak tests will be performed for primary operation at 50 psig. Leak tests will also be performed at 400 psig. Any necessary modifications of the fuel cell components will then be made and the above tests will be repeated. When the fuel cell functionality has been proven, the other components of the assembly will be tested. The Teflon bellows will be tested for leaks and pressure displacement, the base plate for leaks, and the gas cylinders for leaks and mechanical strength at 600 psig. The unit will then be assembled and run as a secondary battery. Because of the internal temperature limitations, the test time will be limited. Complete charge-discharge cycles will be performed with measurement of voltage, current, gas pressure, and external cell temperatures.

8.2 Complite Porosity Study

The test series on the effect of porosity on polarization will be completed so that exact electrode specifications may be included in the next order of porous nickel from Gould National Batteries.

8.3 Safety Investigation

The safety investigations will be continued by repetition of the tests at successively higher pressures to 600 psig and temperatures to 300°F.

8.4 Float Charge Test

A small 1-5/8 inch diameter cell will be assembled for the determination of the effect of float charge on performance. The test will be conducted at JPL.

8.5 Heat Transfer Analysis

The heat transfer analysis of the first prototype will be completed by considering the effects of increasing the number of base plates, as indicated in subsection 5.2, the temperature drop across the cell stack varies inversely as the square of the number of face plates. Variations in load will also be considered. The additional weights associated with the use of the sheaths, and base plates as well as the mechanical problems which might arise will also be determined.

Another heat transfer analysis will then be performed for the case where the fuel cell is located outside the gas cylinders and radiates heat directly to the environment. Although the feasibility of this configuration is dependent upon the elimination of gas leaks, the analysis should be completed.

Finally, an analysis of one final configuration will be made. In this case the fuel cell is again enclosed within the cylinders but its position is shifted so that the outside surface of the cells makes direct contact with the cylinder. A schematic diagram is given:

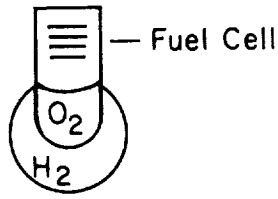

This configuration would eliminate the temperature drop across the cell stack.

8.6 Second Prototype

The results of the above heat transfer analyses, along with considerations of reliability, weight, strength, and ease of assembly and fabrication, will be used for the design of the second prototype. The fuel cell portion of the second prototype will be the same as that of the first if the design is shown to be functional on the first. Perhaps the only change on the fuel cells will be to make the cell spacers thinner.

REFERENCES

1. "Evaluation of Regenerative Fuel Cell" prepared for National Aeronautics and Space Administration, NASA Contract 7-7, EOS Report 1584-Final, p. 19 (April 1962)

2. Hawkins, G.A. and Jakob, M., "Elements of Heat Transfer," John Wiley & Sons, 3rd Edition, p. 109 (1957)

3. Ref. 2 above, p. 106

4. Ref. 2 above, p. 31

APPENDIX

Materials Catalog

Material	Supplier
Asbestos sheet	Braun Chemical Company 1363 S. Bonnie Beach Pl. Los Angeles, Calif.
Potassium hydroxide	Braun Chemical Company 1363 S. Bonnie Beach Pl. Los Angeles, Calif.
Platinum chloride	Braun Chemical Company 1336 S. Bonnie Beach Pl. Los Angeles, Calif.
Silver sheet	Wildberg Bros. Refining Co. 635 South Hill Street Los Angeles, Calif.
Porous nickel sheet	Gould National Batteries 3773 Hillway Drive Glendale, Calif.
Stainless steel fittings Tees, ferrules, valves, caps	W.D. Wilson Company 1118 Mission St. So. Pasadena, Calif.
Plexiglass 55	Cadillac Plastics Company 2305 W. Beverly, Los Angeles, Calif.
Stainless steel plate	Ducommun Metals 4890 S. Alameda St. Los Angeles, Calif.
Stainless steel weld caps	Ducommun Metals 4890 S. Alameda St. Los Angeles, Calif.
Stainless steel tubing	Ducommun Metals 4890 S. Alameda St. Los Angeles, Calif.
Stainless steel pipe	Ducommun Metals 4890 S. Alameda St. Los Angeles, Calif.
O-rings	Robert B. Porter Company 1804 Chiquita Place Glendale, Calif.
Teflon bellows	John L. Dore Company 5406 Schuler Houston, Texas